Cytochrome c_M Decreases Photosynthesis under Photomixotrophy in *Synechocystis* sp. PCC 6803[1][CC-BY]

Daniel Solymosi,[a] Lauri Nikkanen,[a] Dorota Muth-Pawlak,[a] Duncan Fitzpatrick,[a] Ravendran Vasudevan,[b] Christopher J. Howe,[b] David J. Lea-Smith,[b,c] and Yagut Allahverdiyeva[a,2,3]

[a]Laboratory of Molecular Plant Biology, Department of Biochemistry, University of Turku, Turku FI–20014, Finland

[b]Department of Biochemistry, University of Cambridge, Cambridge CB2 1QW, United Kingdom

[c]School of Biological Sciences, University of East Anglia, Norwich NR4 7TJ, United Kingdom

ORCID IDs: 0000-0003-3655-3654 (D.S.); 0000-0002-7192-9322 (L.N.); 0000-0001-7005-2007 (D.M.-P.); 0000-0001-9116-1392 (D.F.); 0000-0001-9195-1116 (R.V.); 0000-0002-6975-8640 (C.J.H.); 0000-0003-2463-406X (D.J.L.-S.); 0000-0002-9262-1757 (Y.A.).

Photomixotrophy is a metabolic state that enables photosynthetic microorganisms to simultaneously perform photosynthesis and metabolism of imported organic carbon substrates. This process is complicated in cyanobacteria, since many, including *Synechocystis* sp. PCC 6803, conduct photosynthesis and respiration in an interlinked thylakoid membrane electron transport chain. Under photomixotrophy, the cell must therefore tightly regulate electron fluxes from photosynthetic and respiratory complexes. In this study, we demonstrate, via characterization of photosynthetic apparatus and the proteome, that photomixotrophic growth results in a gradual inhibition of Q_A^- reoxidation in wild-type *Synechocystis*, which largely decreases photosynthesis over 3 d of growth. This process is circumvented by deleting the gene encoding cytochrome c_M (CytM), a cryptic *c*-type heme protein widespread in cyanobacteria. The ΔCytM strain maintained active photosynthesis over the 3-d period, demonstrated by high photosynthetic O_2 and CO_2 fluxes and effective yields of PSI and PSII. Overall, this resulted in a higher growth rate compared to that of the wild type, which was maintained by accumulation of proteins involved in phosphate and metal uptake, and cofactor biosynthetic enzymes. While the exact role of CytM has not been determined, a mutant deficient in the thylakoid-localized respiratory terminal oxidases and CytM (ΔCox/Cyd/CytM) displayed a phenotype similar to that of ΔCytM under photomixotrophy. This, in combination with other physiological data, and in contrast to a previous hypothesis, suggests that CytM does not transfer electrons to these complexes. In summary, our data suggest that CytM may have a regulatory role in photomixotrophy by modulating the photosynthetic capacity of cells.

Switching between different trophic modes is an advantageous feature that provides great metabolic flexibility for cyanobacteria. For a long time, these photosynthetic prokaryotes were considered to be predominantly photoautotrophic organisms (Smith 1983; Stal and Moezelaar 1997). Lately, accumulating evidence marks the physiological and ecological importance of trophic modes involving organic carbon assimilation, e.g. photomixotrophy (Zubkov and Tarran 2008; Moore, 2013). Dissolved organic carbon, most notably monosaccharides, including Glc and Fru, accumulates in the environment mainly during phytoplankton blooms (Ittekkot et al., 1981; Teeling et al., 2012). During photomixotrophy, photosynthetic organisms must balance the consumption of organic carbon sources with photosynthesis and carbon fixation.

In the model cyanobacterium *Synechocystis* sp. PCC 6803, photomixotrophy is further complicated by the operation of anabolic and catabolic processes occurring in the same cellular compartment and by the presence of an interlinked thylakoid membrane-localized electron transport pathway involved in both photosynthesis and respiration (Vermaas, 2001; Mullineaux, 2014; Lea-Smith et al., 2016a). In *Synechocystis*, photosynthetic linear electron flow is similar to other oxygenic photoautotrophs. In PSII and PSI, the energy of the harvested photons induces charge separation. Electrons from the PSII primary donor P680 pass via pheophytin and the primary quinone Q_A to the secondary quinone, Q_B. Oxidized $P680^+$, which drives water splitting on the luminal side of PSII, is the strongest biological oxidizing molecule. When Q_B is doubly reduced, it binds two

[1]This work was supported by the Academy of Finland (project no. 315119 to Y.A. and Finnish Center of Excellence project no. 307335), the NordForsk Nordic Center of Excellence "NordAqua" (no. 82845), and the Waste Environmental Education Research Trust (C.J.H.).

[2]Author for contact: allahve@utu.fi.

[3]Senior author.

The author responsible for distribution of materials integral to the findings presented in this article in accordance with the policy described in the Instructions for Authors (www.plantphysiol.org) is: Yagut Allahverdiyeva (allahve@utu.fi).

D.S. and Y.A. designed the research; D.S. performed the majority of the experiments; D.M.P. and D.S. performed and analyzed proteomics data; L.N. performed Cyt*f* kinetic measurements and immunoblotting; D.J.L.-S. constructed the mutant strains; all authors contributed to analysis of the data; D.S., Y.A., and D.J.L.-S wrote the article; and all authors revised the manuscript.

www.plantphysiol.org/cgi/doi/10.1104/pp.20.00284

protons from the cytosol, converting plastoquinone (PQ) to plastoquinol (PQH_2), which then diffuses into the membrane PQ pool. Cytochrome (Cyt) b_6f receives two electrons from PQH_2 and transfers an electron to the mobile small protein, plastocyanin (Pc) or cytochrome c_6 (Cyt c_6). An electron is subsequently transferred to PSI, replacing a newly excited electron that is transferred from the PSI reaction center $P700^+$ via several co-factors to ferredoxin (Fed). Lastly, electrons are transferred from Fed to $NADP^+$ by Fed-$NADP^+$ reductase (FNR) to generate NADPH. In the respiratory electron transfer pathway, PQ is reduced by NAD(P)H dehydrogenase-like complex I (NDH-1) and succinate dehydrogenase (SDH), using electrons ultimately derived from Fed (Schuller et al., 2019) and succinate, respectively. Electrons from the PQ pool can be transferred to a thylakoid-localized respiratory terminal oxidase (RTO), cytochrome *bd*-quinol oxidase (Cyd), or, via Cyt b_6f and Pc/Cyt c_6 to a second RTO, an aa_3-type cytochrome *c* oxidase complex (Cox). How *Synechocystis* regulates electron input from PSII and the NDH-1 and SDH complexes into the photosynthetic electron transport chain and to RTOs under photomixotrophic conditions is not fully understood. Moreover, *Synechocystis* encodes four isoforms of the flavodiiron proteins (FDPs), Flv1 to Flv4, which likely utilize NAD(P)H (Vicente et al., 2002; Brown et al., 2019) or reduced Fed (Santana-Sanchez et al., 2019). These proteins function in light-induced O_2 reduction as heterooligomers consisting of Flv1/Flv3 and/or Flv2/Flv4 (Helman et al., 2003; Allahverdiyeva et al., 2013, 2015; Mustila et al., 2016; Santana-Sanchez et al., 2019).

In *Synechocystis*, the water-soluble Cyt c_6 (formerly referred to as Cyt c_{553}) can substitute for Pc under conditions of copper deprivation (Durán et al., 2004). Cyt c_6 belongs to the Cyt *c* family, whose members are characterized by a covalently bound *c*-type heme cofactor. *c*-type Cyts are further classified into groups such as the Cyt c_6-like proteins, Cyt c_{555}, Cyt c_{550}, and CytM (Bialek et al., 2008). Apart from the well-established role of Cyt c_6 in electron transfer (Kerfeld and Krogmann, 1998) and the role of Cyt c_{550} (PsbV) in stabilizing the PSII water splitting complex (Shen and Inoue, 1993), most of the Cyt *c* proteins remain enigmatic.

Cyt c_M (CytM) is conserved in nearly every sequenced cyanobacterium, with the exception of the obligate symbionts *Candidatus acetocyanobacterium thalassa* and *Candidatus Synechococcus spongiarum* (Supplemental Fig. S1; Bialek et al., 2016). In *Synechocystis*, CytM is encoded by *sll1245* (Malakhov et al., 1994). Nevertheless, its subcellular location is ambiguous. An early study localized CytM to the thylakoid and plasma membranes in "purified" membrane fractions (Bernroitner et al., 2009). However, cross contamination between membranes, which has been an issue in studies using similar separation techniques, was not determined (Sonoda et al., 1997; Schultze et al., 2009). In later proteomics studies, CytM has not been detected or localized using membranes purified by either two-phase aqueous polymer partitioning or subcellular fractionation (Baers et al., 2019). However, the structure of the hydrophobic N terminus resembles a signal peptide, which suggests that CytM is targeted to a membrane. Sequence similarity to the N terminus cleavage site of *Synechocystis* Cyt c_6 suggests that the N terminus is processed and the mature 8.3-kD protein is inserted into the lumen (Malakhov et al., 1994). However, cleavage does not seem to occur in vivo, as the protein extracted from various cyanobacterial species, including *Synechocystis*, *Synechococcus elongatus* PCC 6301, and *Anabaena* sp. PCC 7120, was found to be around 12 kD (Cho et al., 2000; Bernroitner et al., 2009), implying that the hydrophobic N terminus remains on the protein and serves as a membrane anchor. The subcellular location of CytM, and whether it is membrane anchored, is therefore still unknown.

It has been suggested that CytM may play a role in respiratory or photosynthetic electron transfer (Manna and Vermaas, 1997; Bernroitner et al., 2009). In *Synechocystis*, CytM was shown to reduce the Cu_A center of Cox in vitro with efficiency similar to that of Cyt c_6 (Bernroitner et al., 2009). However, given the midpoint potential of CytM (+150 mV), electron transfer from Cyt*f* (+320 mV) to CytM would be energetically uphill (Cho et al., 2000). Notably, CytM is unable to reduce PSI in vitro (Molina-Heredia et al., 2002). Thus, it is difficult to see how the protein would substitute for Cyt c_6 or Pc. Importantly, CytM is not detected under photoautotrophic conditions (Baers et al., 2019), and deletion of the gene does not affect net photosynthesis or dark respiratory rates (Malakhov et al., 1994) under these conditions. Cold, high light, and salt stress, however, induce gene expression and the stress-induced cotranscriptional regulation between *cytM* (CytM), *petJ* (Cyt c_6), and *petE* (Pc) suggests a stress-related role in electron transfer (Malakhov et al., 1999).

Besides environmental stresses, CytM has been linked to organic carbon-assimilating trophic modes. A dark-adapted variant of *Leptolyngbya boryana* was found to grow faster than the wild type in heterotrophy. Genome resequencing revealed that the fast-growing strain harbored a disrupted *cytM* (Hiraide et al., 2015). In line with this, the *cytM* deletion mutant of *Synechocystis* demonstrated a growth advantage over the wild type under dark- and light-activated heterotrophic conditions, and under photomixotrophic conditions (Hiraide et al., 2015). Under dark heterotrophic conditions, ΔCytM had higher dark respiration and net photosynthesis. However, the physiological mechanism and the functional role of CytM remain entirely unknown.

In this study, we sought to uncover the bioenergetics of photomixotrophically grown *Synechocystis* and the physiological background behind the growth advantage of ΔCytM by characterizing their photosynthetic machinery and the proteomic landscape. We demonstrate gradual inhibition of Q_A^- reoxidation, resulting in repression of linear electron transport and CO_2 fixation in *Synechocystis* during photomixotrophic growth. A mutant lacking CytM circumvents inhibition

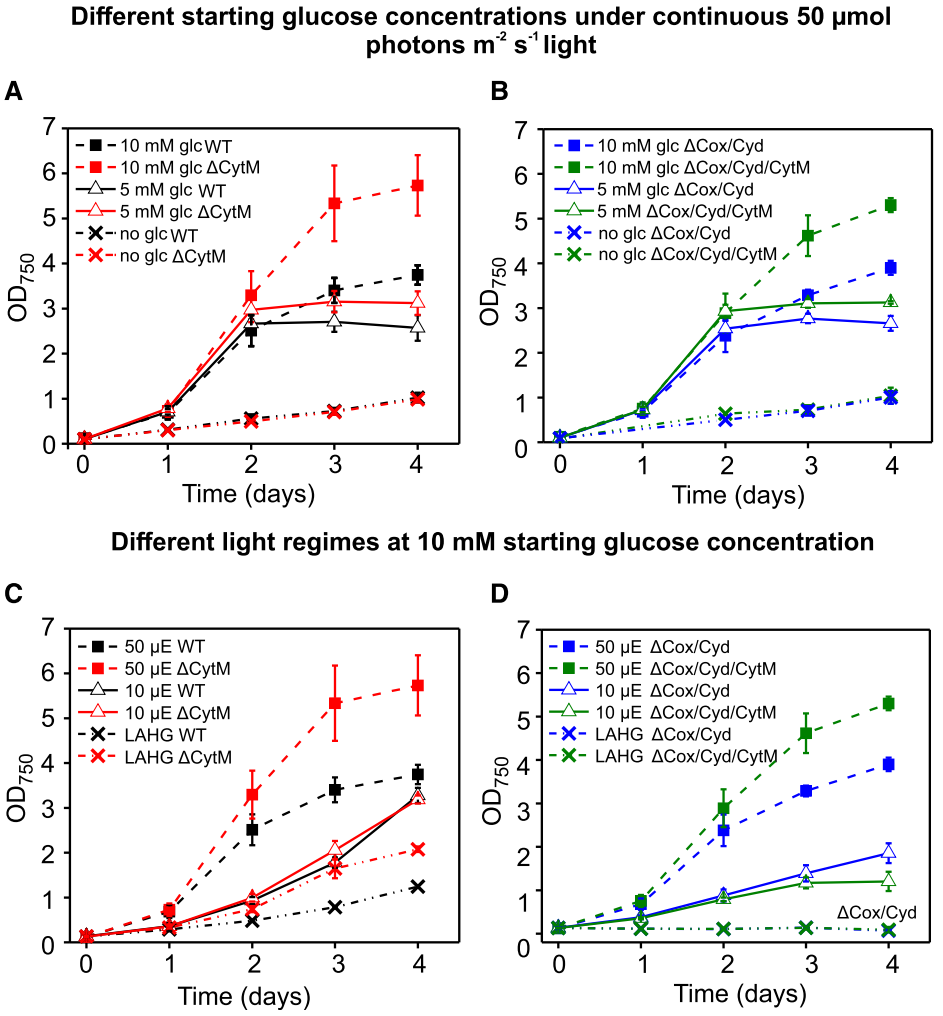

Figure 1. Impact of different Glc concentrations and light regimes on the growth of wild type (WT), ΔCytM, ΔCox/Cyd, and ΔCox/Cyd/CytM. Cultures were exposed to 50 μmol photons m^{-2} s^{-1} light (A and B) and were grown under photoautotrophic conditions without Glc (dash-dotted line) or under photomixotrophic conditions with 5 mM Glc (solid line) or 10 mM Glc (dashed line). Growth was then assessed under various light regimes in cultures containing 10 mM Glc (C and D), under constant 50 μmol photons m^{-2} s^{-1} light (dashed line), constant 10 μmol photons m^{-2} s^{-1} light (solid line), and LAHG, which included 15 min of 50 μmol photons m^{-2} s^{-1} light exposure every 24 h (dash-dotted line). Values are means ± SD, n = 3–7 biological replicates. OD_{750}, Optical density at 750 nm.

of Q_A^- reoxidation during photomixotrophic growth, enabling higher rates of net photosynthesis. In order to meet the substrate demand for enhanced growth, the mutant retains transporter proteins, cofactor biosynthetic enzymes, and slightly adjusts central carbon metabolism compared to the photomixotrophic wild type. Although the function of CytM was previously associated with Cox, both thylakoid respiratory terminal oxidases, Cox and Cyd, were found to be dispensable for the metabolic advantage conferred by deletion of CytM in photomixotrophy. We conclude that when cells are exposed to high Glc conditions, CytM reduces the photosynthetic capacity and contributes to regulation of the redox state of the intertwined photosynthetic and respiratory electron transport chain in order to accommodate this new energy source.

RESULTS

Deletion of CytM Confers a Growth Advantage on ΔCytM and ΔCox/Cyd/CytM in Photomixotrophy

In order to elucidate the physiological role of CytM and its possible functional association with thylakoid-localized RTOs, we studied the Δ*CytM*, Δ*Cox/Cyd*, and Δ*Cox/Cyd/CytM* mutants. Unmarked mutants of *Synechocystis* lacking CytM were constructed by disrupting the *cytM* gene (*sll1245*) in the wild type (Supplemental Fig. S2) and the Δ*Cox/Cyd* mutant (Lea-Smith et al., 2013). Strains were then precultured under photoautotrophic conditions at 3% CO_2 and examined under a range of different growth conditions at air-level CO_2.

First, we determined whether deletion of *cytM* affected photoautotrophic growth by culturing cells under moderate constant 50 μmol photons m^{-2} s^{-1} light. In line with previous studies (Malakhov et al., 1994; Hiraide et al., 2015), no growth difference was observed between ΔCytM and the wild type under photoautotrophic conditions (Fig. 1A).

Next, we characterized growth under photomixotrophic conditions. To determine how different starting Glc concentrations affected photomixotrophic growth (Fig. 1, A and B), we supplemented the medium with 5 mM and 10 mM Glc and cultivated the strains under constant 50 μmol photons m^{-2} s^{-1} light. Based on optical density measurements (OD_{750}), all cultures with added Glc grew substantially faster than those

cultured photoautotrophically (Fig. 1, A and B). Deletion of *cytM* had no effect on cells grown at 5 mM Glc. However, after 3 d of culture with 10 mM Glc, ΔCytM had an OD_{750} 1.9 ± 0.4 (P = 6E−6) times higher than that of the wild type and ΔCox/Cyd/CytM had an OD_{750} 1.9 ± 0.6 (P = 0.002) times higher than that of ΔCox/Cyd. In line with this, ΔCytM consumed more Glc than did the wild type (Fig. 2A), as quantified by measuring the Glc concentration of the cell-free spent media on day 3 of photomixotrophic growth.

We next characterized growth under photomixotrophic conditions but with different light regimes (Fig. 1, C and D), either constant light at 10 μmol photons m^{-2} s^{-1} (low-light photomixotrophy) or 50 μmol photons m^{-2} s^{-1} light for 15 min every 24 h (light-activated heterotrophic growth [LAHG]). These cultures were supplemented with 10 mM starting Glc. Interestingly, under low-light photomixotrophy, neither ΔCytM nor ΔCox/Cyd/CytM demonstrated a growth advantage compared to the wild type and ΔCox/Cyd, respectively. Under the LAHG condition, ΔCytM grew faster than the wild type, as previously reported (Hiraide et al., 2015). The ΔCox/Cyd and ΔCox/Cyd/CytM mutants were unable to grow under LAHG, supporting the findings of Pils (1997), who reported that Cox is indispensable under this condition.

We next examined the morphology of ΔCytM and wild-type cells on day 3 of photomixotrophic growth (10 mM Glc, 50 μmol photons m^{-2} s^{-1} constant light), when the highest difference in OD_{750} was observed. Cell size, cell number per OD_{750}, and chlorophyll (chl) concentration per cell were determined. No difference was observed in cell size between ΔCytM and the wild type (Supplemental Fig. S3), and the cell number per OD_{750} was similar in both strains (Fig. 2B), confirming that the difference in OD_{750} reflects higher growth. However, the chl *a* content per cell increased in ΔCytM (Fig. 2C), suggesting that the photosystem content, or PSII/PSI ratio, has been altered in this strain.

Overall, the most pronounced growth advantage of ΔCytM over the wild type was observed when cells were exposed to a light intensity of 50 μmol photons m^{-2} s^{-1} and Glc concentration of 10 mM. Therefore, these conditions were used for all subsequent phenotyping experiments in which cells cultured photomixotrophically were examined. The same phenotype manifested in the triple ΔCox/Cyd/CytM mutant, showing that Cox and Cyd are not required for the growth advantage. Moreover, we demonstrate that deletion of *cytM* leads to a higher cellular chl *a* content, which implies an altered photosynthetic machinery when cells are cultured photomixotrophically.

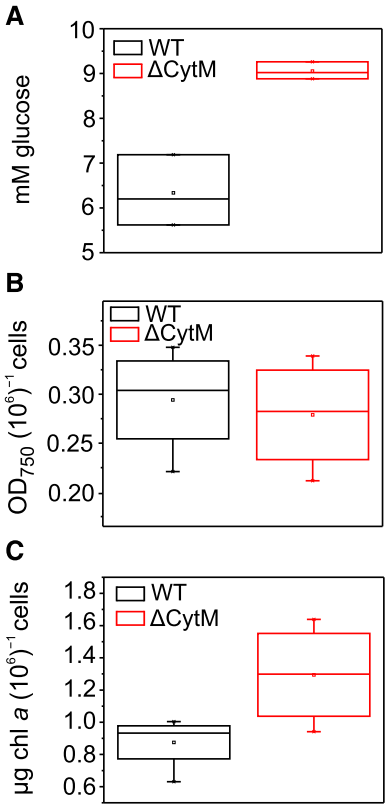

Figure 2. Glc consumption, cellular chl content, and cell number of wild-type (WT) and ΔCytM cultures on day 3 of photomixotrophic growth. A, Amount of Glc consumed by the cells was deduced from the remaining Glc in spent media on day 3. This number reflects the consumption of the whole culture rather than the Glc uptake rate of a given number of cells. B and C, Optical density per cell number (B) and cellular chl content (C) were determined. Values are means ± SD for n = 3 biological replicates. Cultures were grown photomixotrophically under constant 50 μmol photons m^{-2} s^{-1} illumination supplemented with 10 mM Glc. Samples were taken on day 3. OD_{750}, Optical density at 750 nm.

Deletion of CytM Circumvents Inhibition of Q_A^- Reoxidation under Photomixotrophy

To determine how long-term exposure to photomixotrophy affects the photosynthetic machinery of *Synechocystis* wild type and how deletion of CytM rescues this phenotype, we first analyzed net photosynthesis by probing the O_2 evolution capacity of cells (Fig. 3E). When wild-type cells were grown photomixotrophically, only marginal net photosynthetic O_2 evolution was observed on day 3. Strikingly, in the presence of the artificial electron acceptor 2,6-dichloro-*p*-benzoquinone (DCBQ), the O_2 evolving capacity of the photomixotrophically grown wild type increased, although not to the level of the photoautotrophically cultured wild type. DCBQ accepts electrons from Q_A and/or Q_B, disconnecting PSII from the downstream electron transfer chain (Srivastava et al., 1995). This suggests that a high proportion of PSII complexes are functional in the photomixotrophically cultured wild type and that inhibition of net photosynthesis is induced by a blockage downstream of PSII. Photomixotrophically grown ΔCytM demonstrated net photosynthetic O_2 production and PSII activity similar to those of the photoautotrophically cultured wild type,

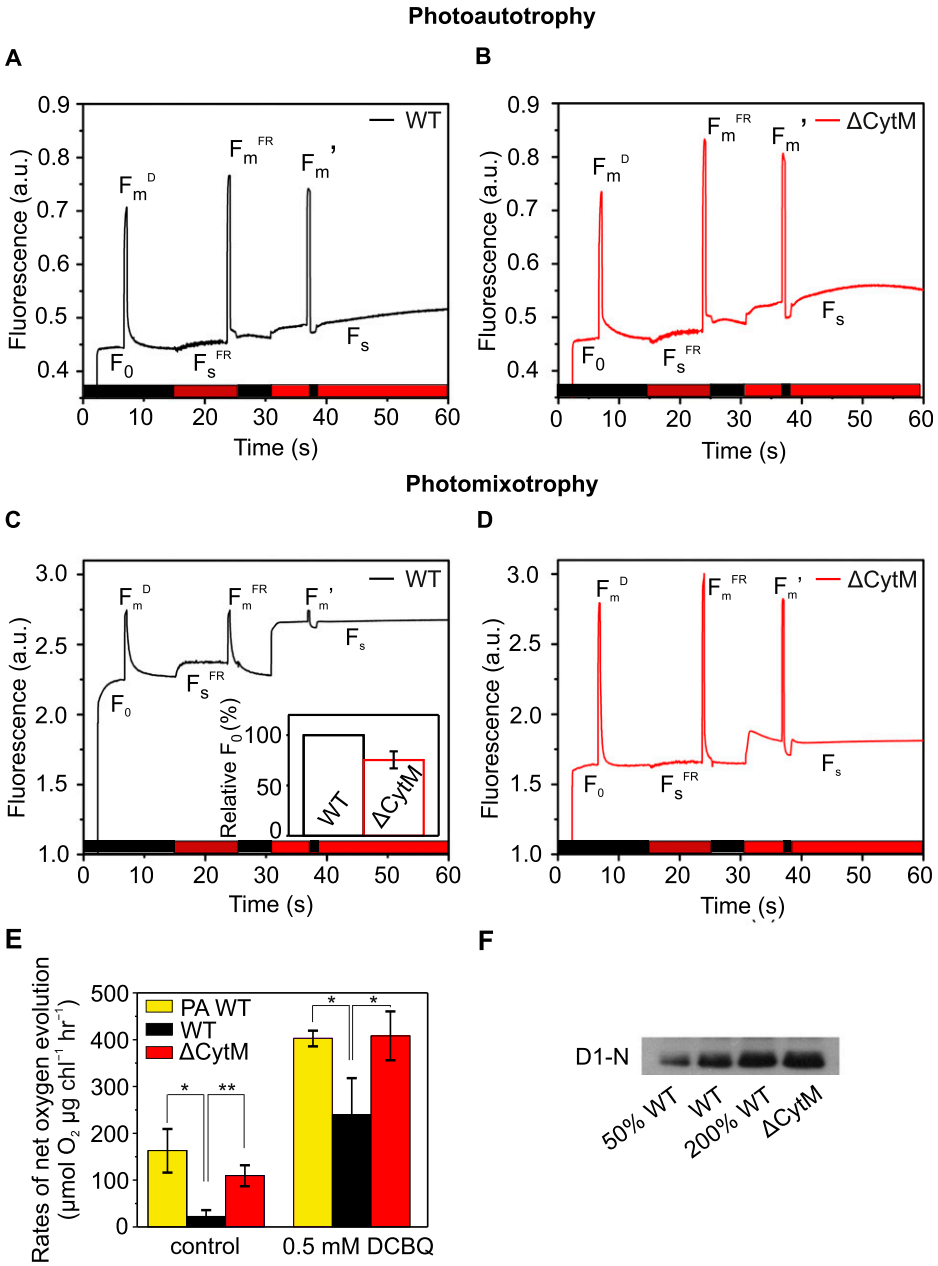

Figure 3. Fluorescence yield in wild-type (WT) and ΔCytM cells and quantification of O_2 production capacity during photomixotrophic growth. A to D, Chl fluorescence of photoautotrophically (A and B) and photomixotrophically (C and D) grown wild-type and ΔCytM whole cells. Photoautotrophic and photomixotrophic cultures were grown under constant 50 μmol photons m^{-2} s^{-1} illumination for 3 d, with or without 10 mM Glc, respectively. Prior to measurements, cells were resuspended in BG-11 with (C and D) and without (A and B) 10 mM Glc and dark adapted for 15 min. Maximum fluorescence was determined by applying a MT saturating pulse (500 ms at 5,000 μmol photons m^{-2} s^{-1}) in darkness (black bars), under 40 W m^{-2} far-red light (brown bars), and under 50 μmol photons m^{-2} s^{-1} actinic red light (red bars). F_0, initial fluorescence; F_m^D, maximum fluorescence in dark; F_m^{FR}, maximum fluorescence in far-red light; F_m', maximum fluorescence in actinic red light; F_s^{FR}, steady-state fluorescence in far-red light; F_s, steady-state fluorescence in actinic red light. E, Rates of net oxygen production of photoautotrophically (PA WT) and photomixotrophically grown wild type and ΔCytM were determined in cells taken on day 3 of growth. O_2 production was initiated with white light (1,000 μmol photons m^{-2} s^{-1}) in the absence (control) and presence of 0.5 mM DCBQ. Rates are expressed as micromoles O_2 per milligram chlorophyll per hour, with the DCBQ-treated wild type considered as 100%. Values are means ± SD for $n = 4$ biological replicates. Asterisks indicate statistically significant differences (*$P < 0.05$ and **$P < 0.001$). F, Immunoblot analysis with D1-N antibody was performed on samples taken on day 3. Fifteen micrograms total protein extract was loaded per 100% lane; 50% and 200% correspond to 7.5 and 30 μg, respectively. a.u., Arbitrary units.

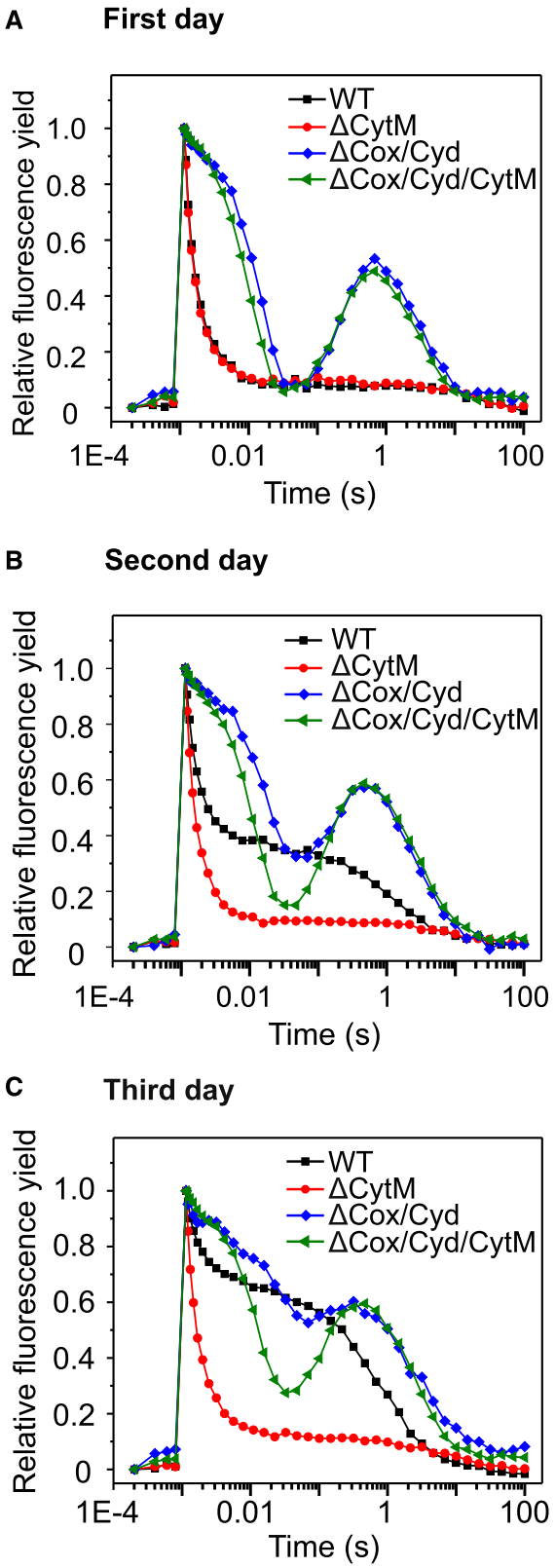

Figure 4. Relaxation of flash-induced fluorescence yield in cells exposed to darkness. Subsequent relaxation of fluorescence yields in the dark was measured after a single-turnover saturating pulse in photomixotrophically cultured cells taken on days 1 (A), 2 (B), and 3 (C) of cultivation. Growth conditions are described in Figure 3. Prior to measurements, the cell suspension was adjusted to 5 μg chl mL^{-1}, resuspended in BG-11 supplemented with 10 mM Glc, and dark adapted for 5 min. WT, Wild type.

implying that deletion of CytM preserves photosynthetic activity under photomixotrophy. Immunoblotting performed on total protein extracts from the photomixotrophically grown wild type and ΔCytM demonstrated a higher accumulation of PSII reaction center protein D1 in CytM compared to the former (Fig. 3F), suggesting that PSII levels are maintained in the mutant throughout photomixotrophic growth. The increased amount of D1 in ΔCytM likely contributes to the higher O_2 production in this mutant compared to the wild type, although it is unlikely to entirely account for the difference.

Next, we assessed photosynthetic activity by probing chl fluorescence in wild-type and ΔCytM whole cells with multiple-turnover (MT) saturating pulses in the dark and under far-red and actinic red light (Fig. 3, A–D). Compared to ΔCytM cells cultured photoautotrophically (Supplemental Fig. S4A), wild-type cells grown photomixotrophically demonstrated substantially higher initial fluorescence (F_0) and slower relaxation of pulse-induced fluorescence in the dark (see F_m^D relaxation in Fig. 3C), which suggests that the PQ pool is highly reduced. To verify this, cells were exposed to far-red light, which preferentially excites PSI, resulting in oxidation of the PQ pool. If the PQ pool is highly reduced, one would expect a lower steady-state fluorescence level (F_s) upon illumination of the cells with far-red light, similar to that observed in the ΔCox/Cyd mutant (Ermakova et al., 2016). Interestingly, the opposite effect, a considerable increase in F_s^{FR}, was observed (Fig. 3C). This increase suggests that inhibition of electron transport occurs at Q_B, since the negligible actinic effect of far-red light is sufficient to reduce Q_A, resulting in increased fluorescence. Indeed, a similar rise in fluorescence was observed in photoautotrophically cultured wild-type cells measured in the presence of 3-(3,4-dichlorophenyl)-1,1-dimethylurea (DCMU; Supplemental Fig. S4C), a chemical occupying the Q_B site, thus blocking Q_A-to-Q_B forward electron transfer in PSII.

Moreover, the F_s level under steady-state actinic light was considerably higher compared to cells grown photoautotrophically, and firing saturating pulses barely increased fluorescence (see F_m' in Fig. 3C), implying a highly reduced Q_A and negligible effective PSII yield [Y(II); Supplemental Fig. S5A]. Similar results were observed in a different wild-type *Synechocystis* substrain commonly used in our laboratory (Supplemental Fig. S6) and in cells exposed to longer periods of illumination (Supplemental Fig. S7A). Taken together, these results suggest a limited capacity to oxidize the PSII acceptor site, i.e. Q_A, in photomixotrophically cultured wild-type cells under illumination.

Compared to the photomixotrophically grown wild type, ΔCytM cultured under the same conditions demonstrated 24.8% ± 8.3% lower F_0 and the pulse-induced fluorescence relaxation in darkness was markedly faster (see F_m^D in Fig. 3D). Far-red illumination did not increase fluorescence, while saturating pulses greatly increased it (see F_m' in Fig. 3D), suggesting that the PSII effective yield, Y(II), remained significantly higher, unlike in photomixotrophically grown wild-type cells (Supplemental Fig. S5A). Thus, in sharp contrast to the wild type, ΔCytM preserved a well-oxidized electron transport chain under photomixotrophy. Similarly, the triple mutant ΔCox/Cyd/CytM demonstrated high Y(II) compared to ΔCox/Cyd under photomixotrophy (Supplemental Figs. S7, C and D, and S8, C and D).

To determine how the wild type builds up a highly reduced Q_A over 3 d of photomixotrophic growth, we monitored the redox kinetics of the PSII primary electron acceptor Q_A (Fig. 4) by firing a single-turnover saturating flash on dark-adapted cells. Relaxation of the chl fluorescence yield was then recorded in the period of subsequent darkness. No difference was observed between wild-type and ΔCytM cells cultured photoautotrophically (Supplemental Fig. S9A), and on the first day of photomixotrophy, both wild-type and ΔCytM cells demonstrated typical flash-fluorescence relaxation in the darkness. On day 2, wild-type cells demonstrated a substantial slow-down in Q_A^- reoxidation, reflected by slow decay kinetics (Fig. 4B), while on day 3, there was a nearly complete loss of Q_A-to-Q_B electron transfer (Fig. 4C).

Interestingly, the kinetics from day 3 resembled a curve recorded in the photoautotrophically cultured wild type supplemented with DCMU prior to measurement (Supplemental Fig. S9A). This supports the conclusion that Q_A-to-Q_B electron transfer was strongly inhibited in the majority of PSII centers in the wild type on the third day of photomixotrophy. Preillumination of the cells with far-red light did not accelerate Q_A^- reoxidation (Supplemental Fig. S9B), thus supporting the idea that the inhibition is not simply due to a highly reduced PQ pool, although overreduction of the PQ pool cannot be excluded.

ΔCox/Cyd and ΔCox/Cyd/CytM displayed pronounced waving in the fluorescence yield relaxation kinetics (Fig. 4). The wave phenomenon is an unusual pattern in the decay of flash-induced chl fluorescence yield in the dark. The feature is characterized by a dip, corresponding to transient oxidation of Q_A^-, and a subsequent rise, reflecting rereduction of the PQ pool by NDH-1 (Deák et al., 2014). During growth over the 3-d period, the wave phenomenon in ΔCox/Cyd became less evident due to gradual inhibition of Q_A-to-Q_B electron transfer. In contrast, ΔCox/Cyd/CytM displayed prominent waving during all 3 d of photomixotrophic growth, demonstrating that Q_A^- reoxidation was sustained. Slight waving in ΔCox/Cyd under photoautotrophic conditions was reported previously (Ermakova et al., 2016), and here we demonstrate that Glc induces a strong wave phenomenon.

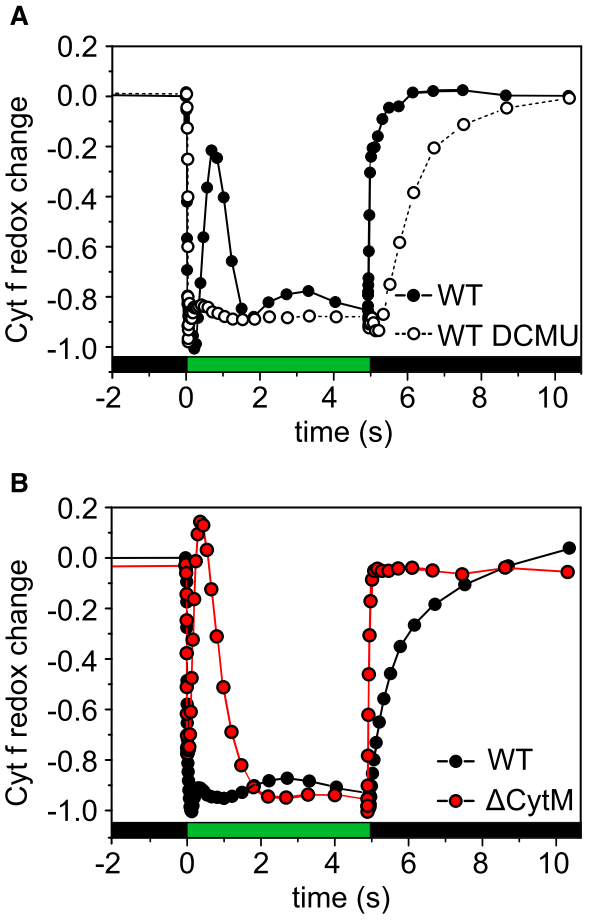

Figure 5. Redox kinetics of Cyt *f* in wild-type (WT) and ΔCytM cells. Cells were grown for 3 d under photoautotrophic (A) and photomixotrophic (B) conditions, as described in Figure 3. Oxidation of Cyt *f* was induced by 500 μmol photons m^{-2} s^{-1} green light. When indicated, 20 μM DCMU was added prior to the measurement. The curves were normalized to their respective maximal oxidation. The kinetics are representative of three biological replicates.

In order to evaluate electron transfer through Cyt b_6f, the redox kinetics of Cyt *f* were examined (Fig. 5). Both the photoautotrophically grown wild type (Fig. 5A) and ΔCytM (Supplemental Fig. S10) demonstrated fast oxidation of Cyt *f* followed by its reduction and reoxidation, exhibiting wavelike kinetics upon dark-to-light transition. In the subsequent dark, rapid reduction of Cyt *f* was observed. When DCMU was added to the wild type prior to the measurement (Fig. 5A), illumination initiated steady oxidation, but the transient rereduction was eliminated and the subsequent reduction in dark was slower. The photomixotrophically grown wild type (Fig. 5B) demonstrated trends similar to DCMU-treated wild-type cells grown under photoautotrophic conditions, confirming that electron transfer from PSII to Cyt b_6f is inhibited. In contrast, ΔCytM grown photomixotrophically (Fig. 5B) resembled

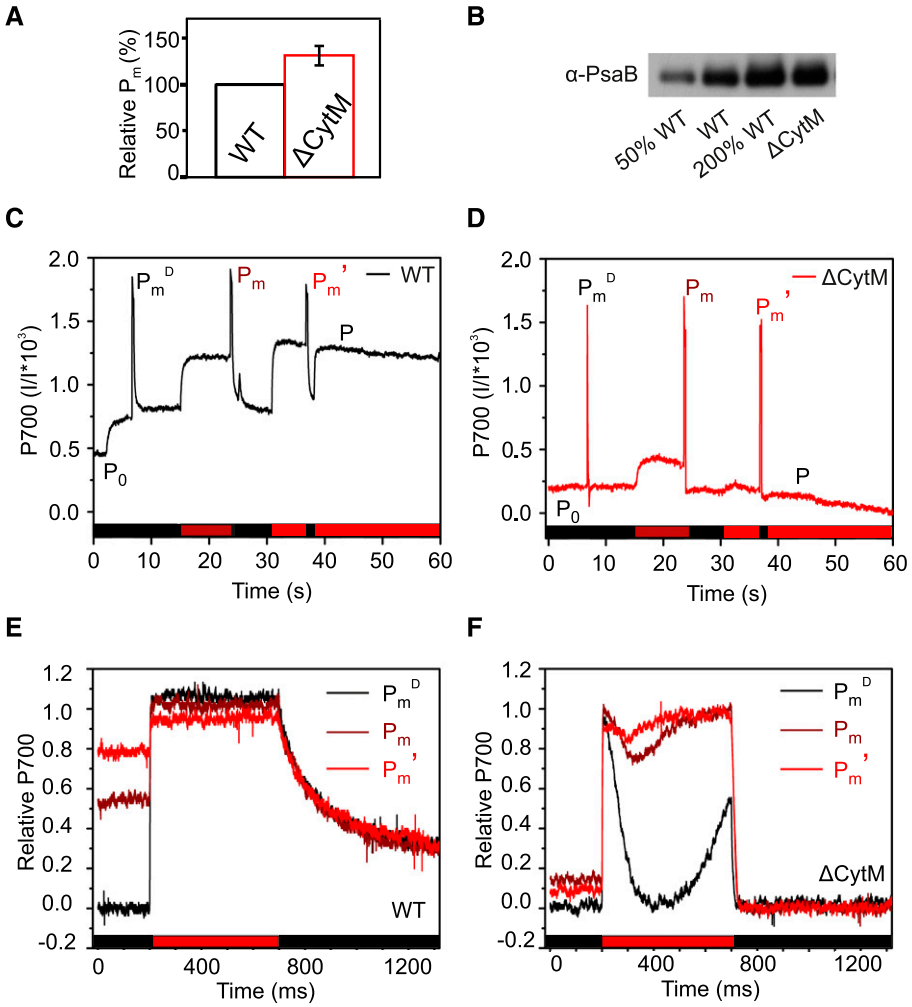

Figure 6. Characterization of PSI in cells cultured photomixotrophically. The maximal amount of oxidizable P700, P_m (A), and immunoblotting of the PSI reaction center protein PsaB (B) were determined in cells cultured photomixotrophically. Values are means ± SD for $n = 3$ biological replicates. C to F, Slow (C and D) and fast (E and F) kinetics were measured in parallel with fluorescence (Fig. 3). Fast kinetics curves are normalized to P_m and referenced against their respective minimum P700 signal detected after the pulse. Cultivation, sample preparation, and experimental parameters are similar to those detailed in Figure 3. P_0, Initial P700; P_m^D, maximum P700 in darkness; P_m, maximum P700 under far-red light; P_m', maximum P700 under red actinic light; WT, wild type.

untreated wild-type cells subjected to photoautotrophic conditions.

These results demonstrate that during photomixotrophic growth, the electron flow at the PSII acceptor site gradually becomes inhibited in the wild type, leading to drastically slower electron transfer from PSII to Cyt b_6f on day 3. Deletion of CytM circumvents this inhibition and maintains PSII reaction center protein D1 amounts and a steady electron flux from PSII to Cyt *f*.

ΔCytM Has a Larger Pool of Oxidizable PSI Than the Wild Type under Photomixotrophy

Next, we determined activity of PSI by monitoring the redox kinetics of P700, the primary electron donor of PSI (Fig. 6), which was performed simultaneously with chl fluorescence measurements (Fig. 3). First, the maximal amount of oxidizable P700, P_m, was determined (Fig. 6A). Compared to cells cultured under photoautotrophic conditions, wild-type cells grown photomixotrophically had 45.2% ± 0.03% lower P_m. However, the difference between ΔCytM cultured under photomixotrophic and photoautotrophic conditions was negligible (17.2% ± 19.3%). Thus, under photomixotrophic conditions, the maximum amounts of oxidizable P700 were 132% ± 18.7% higher in ΔCytM than in the wild type (Fig. 6A). In line with this, immunoblotting revealed higher levels of PSI reaction center subunit PsaB in ΔCytM compared to the wild type under photomixotrophic growth (Fig. 6B). To determine the PSI:PSII ratio, samples were analyzed at 77K by measuring chl fluorescence emission. No statistical difference was observed between the wild type and ΔCytM (Supplemental Fig. S11), demonstrating that the PSII:PSI ratio was similar in both strains.

The PSI effective yield, Y(I), was also quantified, and was three times lower in photomixotrophically cultured wild-type cells compared to those grown photoautotrophically (Supplemental Fig. S5B). This is due to a strong donor side limitation of PSI [Y(ND); Supplemental Fig. S5C], which demonstrates an electron shortage to $P700^+$. In contrast, photomixotrophically cultured ΔCytM demonstrated similar Y(I) and only slightly increased Y(ND) compared to photoautotrophically cultured wild type and ΔCytM (Supplemental Fig. S5, B and C). As a result, Y(I) was more than three

times higher in ΔCytM than in the wild type under photomixotrophy (Supplemental Fig. S5B).

Next, pulse-induced P700 fast kinetics were compared between the photoautotrophically and photomixotrophically cultured wild type (Fig. 6E) and ΔCytM (Fig. 6F). These fast kinetics reveal the dynamics of P700 oxidoreduction during saturating pulses on the millisecond scale. Saturating pulses are flashed in darkness (P_m^D) under far-red light (P_m) and actinic red light (P_m'). Typically, the photoautotrophically cultured wild type (Supplemental Fig. S12A) demonstrates transient $P700^+$ rereduction during light pulses. However, the photomixotrophically grown wild type did not exhibit the typical transient rereduction (Fig. 6E). Importantly, $P700^+$ relaxation after the pulse (Fig. 6E) was markedly slower compared to that observed in photoautotrophically cultured cells (Supplemental Fig. S12A). Collectively, these results confirm that fewer electrons were transferred to $P700^+$, leading to a higher Y(ND) in the photomixotrophically grown wild type. Photomixotrophically cultured ΔCytM (Fig. 6F) displayed transient rereduction during the pulses (see P_m^D, P_m^{FR} and P_m' in Fig. 6F) and rapid relaxation after the pulse (Fig. 6F), resembling the photoautotrophically cultured ΔCytM and wild type (Supplemental Fig. S12, A and B).

Here, we have shown that the effective yield of PSI in photomixotrophically cultured wild-type cells was considerably lower compared to photoautotrophically cultured cells due to an electron shortage at $P700^+$. This phenotype is eliminated by deleting *cytM*, as increased Y(I) and higher amounts of oxidizable P700 (P_m) and PsaB were observed in ΔCytM compared to the wild type on day 3 of photomixotrophy.

ΔCytM and ΔCox/Cyd/CytM Sustain Efficient Net Photosynthesis and CO_2 Fixation under Photomixotrophy

To analyze real-time gas exchange in the photomixotrophically grown wild type, ΔCytM, ΔCox/Cyd, and ΔCox/Cyd/CytM (Fig. 7), whole-cell fluxes of O_2 and CO_2 were simultaneously monitored using membrane inlet mass spectrometry (MIMS). In contrast to a classical oxygen electrode, which only determines net O_2 changes, MIMS, via enrichment of the samples with the stable $^{18}O_2$ isotopologue, makes it possible to simultaneously measure the rates of gross $^{16}O_2$ production by PSII and $^{18}O_2$ consumption mediated by FDPs (Flv1–Flv4) and RTOs (Ermakova et al., 2016; Santana-Sanchez et al., 2019). Net O_2 fluxes were calculated by finding the difference between gross rates of $^{16}O_2$ production and $^{18}O_2$ consumption. Furthermore, light-induced O_2 consumption was calculated by subtracting the rate of $^{18}O_2$ consumption in the dark from that in the light.

Although Rubisco fixes CO_2, and the instrument can only measure the concentration of CO_2 in a sample, cells consume both CO_2 and HCO_3^- from the medium. The pH-dependent equilibrium between CO_2 and HCO_3^- makes it possible to calibrate the CO_2 concentration measured with MIMS to the total inorganic carbon (C_i) concentration in the sample. Based on the assumption that during steady-state photosynthesis the consumption of total C_i is a function of Rubisco activity (Badger et al., 1994; Sültemeyer et al., 1995), the total C_i flux represents CO_2 consumption rates.

In the wild type under 200 μmol photons m^{-2} s^{-1}-white light, O^2 consumption and gross production rates were similar, resulting in nearly zero net photosynthetic O_2 production. This is in line with the data obtained by the O_2 electrode (Fig. 3E). Corresponding to the minor net photosynthetic O_2 production observed, the rate of CO_2 consumption was negligible (Fig. 7A; Supplemental Fig. S13A). Importantly, no light-induced O_2 consumption was observed in the wild type (Fig. 7, A and C), although a substantial amount of Flv3 was detected by immunoblotting (Fig. 7B). While the thylakoid-localized RTOs, Cox and Cyd, were shown to be active in light (Ermakova et al., 2016), a slight inhibition of respiratory O_2 consumption occurred in the wild type under 200 μmol photons m^{-2} s^{-1} illumination. In contrast, ΔCytM exhibited a positive net O_2 production rate and active CO_2 consumption (Fig. 7, A and E; Supplemental Fig. S13C). Strikingly, gross O_2 production was ~10 times higher than in the wild type, and $^{18}O_2$ consumption in light followed a triphasic pattern, a characteristic trend reflecting the contribution of Flv1/Flv3 and Flv2/Flv4 to O_2 consumption in light (Santana-Sanchez et al., 2019). The triphasic pattern in ΔCytM was observed as an initial burst of O_2 consumption following the dark-to-light transition, which faded after 1 to 1.5 min and continued at a relatively constant rate (Fig. 7E). Accordingly, immunoblotting confirmed higher accumulation of the Flv3 proteins in ΔCytM. The rate of light-induced O_2 consumption in ΔCytM is comparable to the reported values of the photoautotrophically grown wild type (Huokko et al., 2017; Santana-Sanchez et al., 2019). The dark respiration rate was slightly higher in ΔCytM compared to the wild type, as previously observed in ΔCytM cultured under dark, heterotrophic conditions (Hiraide et al., 2015).

Similar to the wild type, ΔCox/Cyd (Fig. 7, A and D) showed minimal photosynthetic activity on day 3 of photomixotrophic growth. During illumination, net O_2 production remained negative, and CO_2 consumption was found to be negligible (Fig. 7A; Supplemental Fig. S13B). Only residual gross O_2 production was observed, and O_2 consumption was not stimulated by light (Fig. 7, A and D). Flv3 protein abundance in ΔCox/Cyd was comparable to that in the wild type (Fig. 7B). In sharp contrast to ΔCox/Cyd, ΔCox/Cyd/CytM demonstrated high PSII activity and a net O_2 production rate similar to that of ΔCytM (Fig. 7, A and F). ΔCox/Cyd/CytM displayed a triphasic O_2 consumption pattern under illumination (Fig. 7F), and the light-induced O_2 consumption was comparable to that of ΔCytM in steady state (Fig. 7E). Compared to ΔCox/Cyd, ΔCox/Cyd/CytM had higher levels of Flv3 (Fig. 7B). Notably, deleting *cytM* in the ΔCox/Cyd mutant did not enhance dark respiration, whereas ΔCytM had higher rates compared to the wild type.

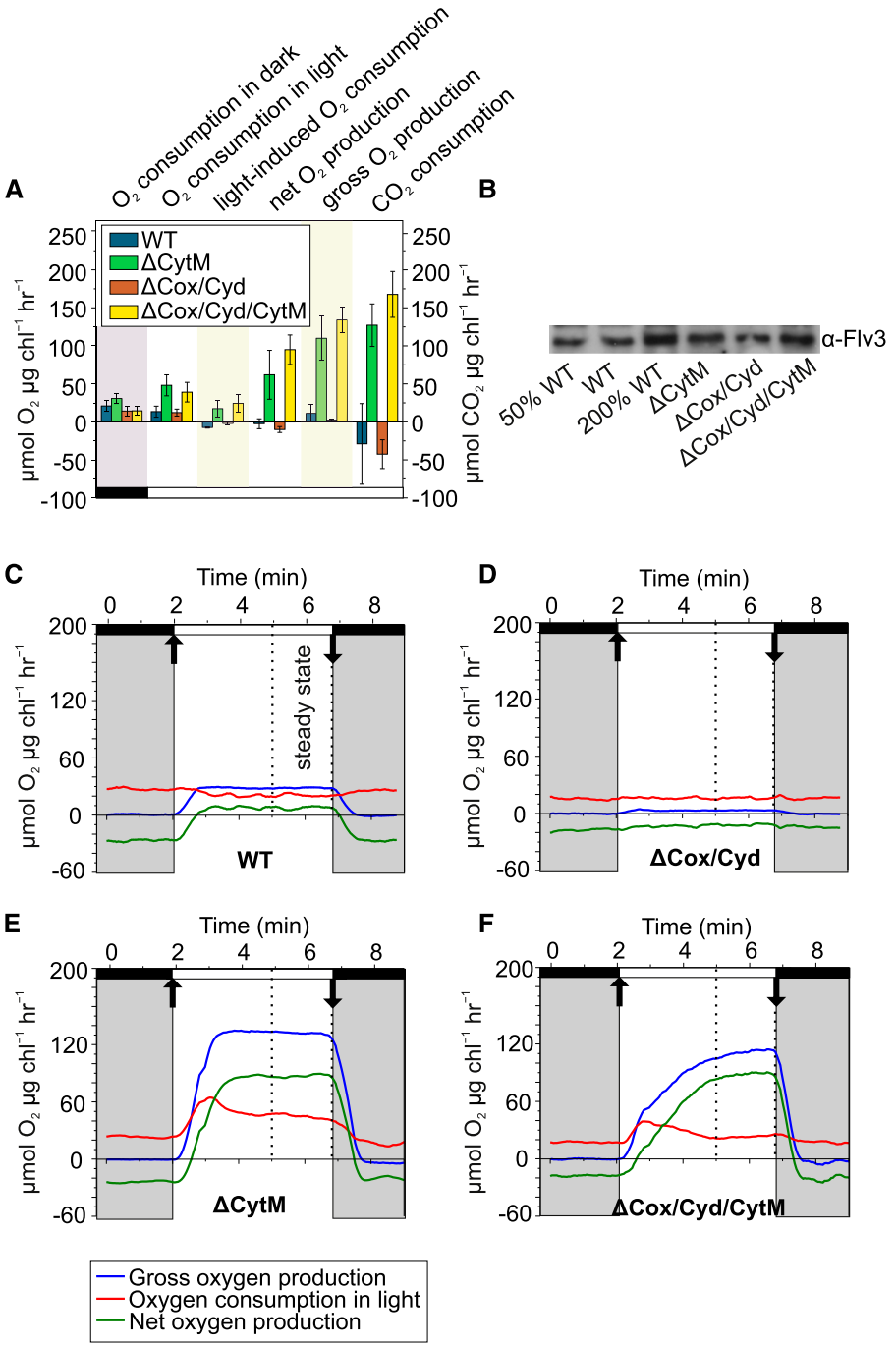

Figure 7. O_2 and CO_2 fluxes in photomixotrophically cultured wild-type (WT), ΔCytM, ΔCox/Cyd, and ΔCox/Cyd/CytM cells. A, Rates of O_2 and CO_2 fluxes at steady state. Values are means ± SD for n = 3 to 5 biological replicates. B, Total protein extracts were analyzed by immunoblotting with α-Flv3-specific antibody: 15 μg total protein was loaded per 100% lane; 50% and 200% correspond to 7.5 μg and 30 μg, respectively. C to F, Kinetics of O_2 flux rates in whole cells. Cultivation, sample preparation, and experimental conditions are detailed in Figure 3. In the light phase, 200 μmol photons m^{-2} s^{-1} constant white light was applied. Samples were supplemented by 1.5 mM $NaHCO_3$. Kinetics are representatives of three to six biological replicates. The source data for Figure 7A can be found in Supplemental Table S2.

To conclude, mutants lacking CytM sustained a steady electron flux toward O_2 and CO_2 under photomixotrophy, reflected by substantial net O_2 production and active CO_2 consumption during illumination.

Photomixotrophically Cultured ΔCytM Cells Accumulate Transport Proteins and Cofactor Biosynthetic Enzymes

In order to understand the metabolism of photomixotrophically grown wild type and ΔCytM, we analyzed the total proteome by nanoscale liquid chromatography electrospray ionization tandem MS via the data-dependent acquisition method. Samples for analysis were collected on day 2, when both wild-type and ΔCytM cells were in the late exponential phase and a substantial growth difference was observed between the strains (Fig. 8A).

In total, 2,415 proteins were identified (Supplemental Dataset S1), despite the fact that the dataset was slightly biased against basic (Fig. 8D) and hydrophobic proteins (Fig. 8E), which is a known issue with this technique (Chandramouli and Qian, 2009). Out of 2,415 proteins,

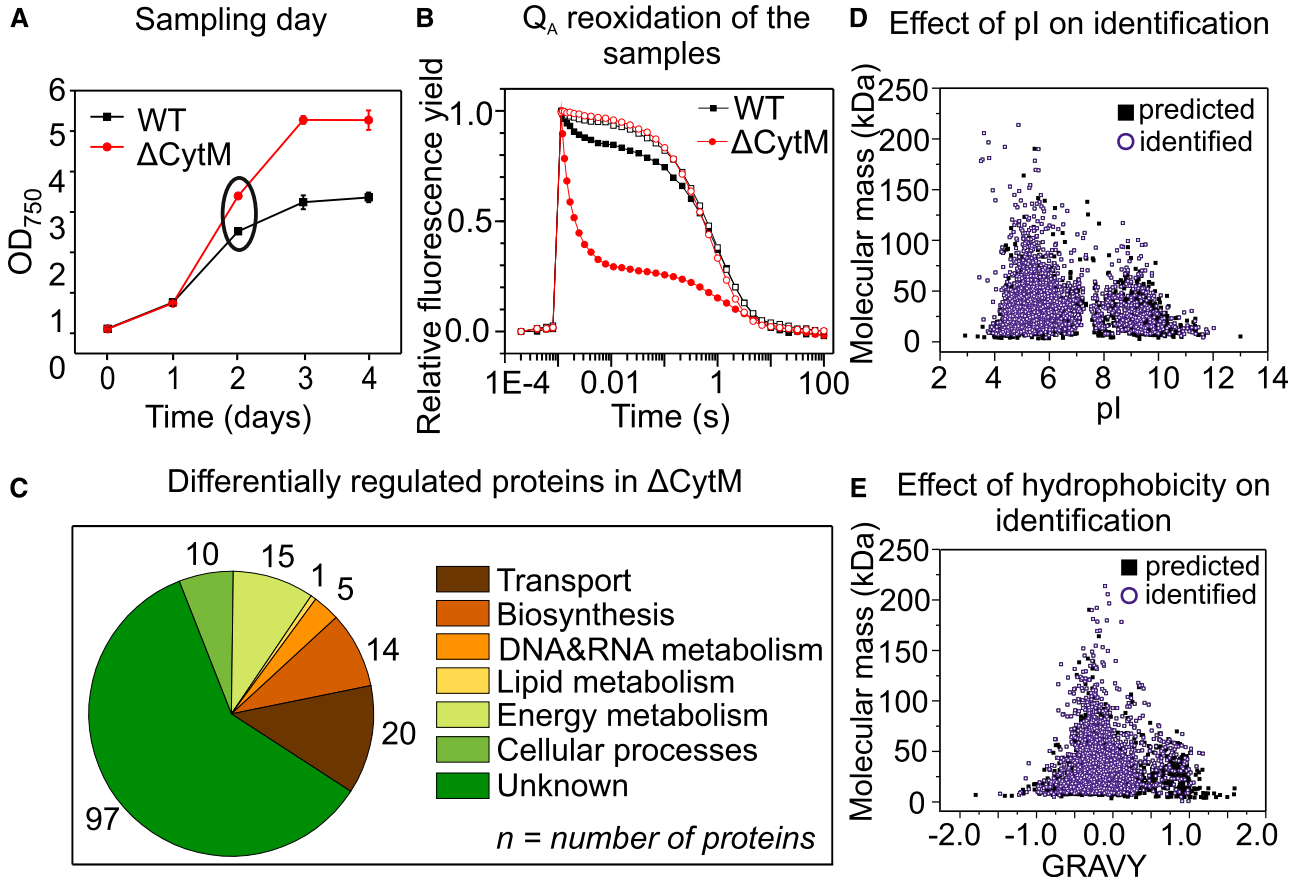

Figure 8. Characteristics at the sampling stage and functional classification of differentially regulated proteins in ΔCytM. A, Growth of the analyzed cultures, with the ellipsis marking the sampling day. Cells were cultured similarly to those used in the biophysics analysis, except that the cells for proteomics were precultivated under atmospheric CO_2 in order to fully adapt the cells to these conditions. Importantly, the extra preculturing step did not affect the growth of the experimental cultures. Values are means ± SD for $n = 3$ biological replicates. B, Relaxation of the flash-induced fluorescence yield in the dark was measured in the absence (solid symbols) and presence (open symbols) of 20 μM DCMU. C, Differentially regulated proteins in ΔCytM were grouped according to their function. In total, 2,415 proteins were identified, of which 634 proteins were quantified and 162 were differentially regulated. The practical significance of differentially regulated proteins was set to FC > 1.5 and FC < -1.5 ($P < 0.05$). D and E, Effects of pI (D) and hydrophobicity (GRAVY; E) of the proteins on the identification rate were determined. Black squares mark all of the 3,507 predicted proteins in *Synechocystis*; lilac circles mark each protein identified in the wild type (WT) and ΔCytM.

634 were quantified, with 162 displaying a statistically different abundance in ΔCytM compared to the wild type (fold change [FC] > 1.5 and FC < -1.5 [$P < 0.05$]; Supplemental Dataset S2). The functional classification of differentially regulated proteins (Fig. 8C) revealed that apart from unknown or hypothetical proteins, mainly transporters and biosynthetic enzymes were altered in photomixotrophically cultured ΔCytM cells.

Supplemental Dataset S3 shows a selection of proteins whose abundance was different in ΔCytM compared to the wild type. The highest fold change was observed in transport proteins. Among these, the constitutive low-affinity ABC-type phosphate transporters (PstA1, PstB1, PstB1′, and PstC), periplasmic phosphate-binding proteins (SphX and PstS1), and extracellular lytic enzymes (PhoA and NucH) were more abundant in ΔCytM. Among proteins related to C_i uptake, a thylakoid β-type carbonic anhydrase, EcaB, was 2.32 times (P = 7.50E−03) more abundant in ΔCytM. EcaB is a CupA/B-associated protein proposed to regulate the activity of NDH-1_3 (NDH-1 MS) and NDH-1_4 (NDH-1 MS′; Sun et al., 2018). NDH-1_3 facilitates inducible CO_2 uptake, whereas NDH-1_4 drives constitutive CO_2 uptake (Ogawa, 1991). CupB is exclusively found in the NDH-1_4 complex and converts CO_2 into HCO_3^-. Interestingly, no significant change was observed in the level of the Glc transporter GlcP, although the growth advantage of ΔCytM was observed upon exposure to Glc.

Chl *a* biosynthetic enzymes were found to accumulate in the mutant (Supplemental Dataset 3). ChlL, a subunit of the light-independent protochlorophyllide reductase (Wu and Vermaas 1995), and ChlP (4.61E−03), a geranylgeranyl reductase (Shpilyov et al., 2005),

were upregulated 9.28-fold (P = 5.32E−03) and 1.52-fold (P = 4.61E−03), respectively, in ΔCytM. Incorporation of chl into photosystems is likely increased due to the elevated level of Pitt, a protein contributing to the formation of photosynthetic pigments/proteins at the early stages of biogenesis (Schottkowski et al., 2009). The ligand of the tetrapyrrole ring of chl is Mg^{2+}, and accordingly, the magnesium uptake protein MgtE accumulated in ΔCytM along with a periplasmic iron-binding protein, FutA2, part of the complementary uptake system of iron, a vital element of the photosynthetic machinery (Kranzler et al., 2014). Among pigment biosynthetic enzymes, ΔCytM showed increased levels of the heme oxygenase Ho1, catalyzing the final step in the production of biliverdin (Willows et al., 2000). Biliverdin is the precursor of phycocyanobilin, which is incorporated into phycobilisomes, the light-harvesting complexes of *Synechocystis*.

Among the photosynthetic proteins, the PSI reaction center subunit PsaB was found in equal amounts in the wild type and ΔCytM. However, immunoblotting with an anti-PsaB antibody demonstrated that ΔCytM contained higher amounts of PsaB than the wild type (Fig. 6B). This discrepancy may be due to the fact that despite the robustness of the MS-based data-dependent acquisition method, hydrophobic membrane proteins are prone to misquantification. Via MS analysis, quantification of *psbA*-encoded D1 was not successful. Therefore, its abundance was only determined by immunoblotting (Fig. 3F), which revealed higher levels of D1 proteins in ΔCytM compared to the wild type. Interestingly, and somewhat contradictorily, the number of PSII assembly proteins encoded by the PSII assembly proteins operon (Wegener et al., 2008) decreased in the mutant. We also note that lower levels of NorB, a quinol-oxidizing nitric oxide reductase (Büsch et al., 2002), were observed in ΔCytM.

Since the growth advantage of ΔCytM was observed in the presence of Glc, alterations are expected in the abundance of the intermediary carbon metabolic enzymes. In *Synechocystis*, ~100 enzymes participate in this metabolic network. In our study, 40 were quantified, and surprisingly, only a few proteins were differentially regulated in ΔCytM. One notable example is phosphofructokinase PfkA, the key regulatory enzyme of the glycolytic Embden-Meyerhof-Parnas pathway, which was 1.86 times (P = 1.96E−05) less abundant in ΔCytM, suggesting that carbon flux might be redirected into the Entner-Doudoroff or oxidative pentose phosphate pathways. Phosphoglycerate kinase Pgk, which is involved in each glycolytic pathway, was 2.06 times (P = 1.27E−05) as abundant in ΔCytM. Phosphoenolpyruvate synthetase PpsA, a protein that catalyzes the first step of gluconeogenesis, was 2.21 times (P = 3.10E−04) less abundant in ΔCytM.

To conclude, global proteomic analysis revealed that photomixotrophically cultured ΔCytM accumulates transporter and chl biosynthetic proteins, while slight changes in the amount of certain glycolytic and photosynthetic proteins were also observed.

DISCUSSION

The effect of importing and metabolizing organic carbon on the bioenergetics properties of cyanobacteria over a long-term period is not fully understood. Previous studies have focused on the cellular changes following relatively short-term (from 10 min to 24 h) exposure to organic carbon (Lee et al., 2007; Takahashi et al.. 2008; Haimovich-Dayan et al., 2011; Zilliges and Dau, 2016). The majority of these reports suggest partial inhibition of photosynthetic activity, whereas some studies demonstrated increased net photosynthesis under air-level CO_2 after 2 h exposure to 10 mM Glc (Haimovich-Dayan et al., 2011). However, long-term changes to bioenergetics processes, particularly photosynthesis, remain to be elucidated. In this study, we investigated the effect of long-term photomixotrophic growth on wild-type and ΔCytM cells, most notably on the photosynthetic machinery, by analyzing chl fluorescence, the redox kinetics of P700, real time O_2 and CO_2 fluxes, and changes within the proteome.

Gradually Disconnecting PSII from Cytb_6f Limits Photosynthesis in the Photomixotrophically Cultured Wild Type

By characterizing wild-type cells shifted from photoautotrophic to photomixotrophic conditions, we show that photosynthesis was markedly decreased over 3 d of cultivation. This is deduced from the low PSII (Fig. 3C; Supplemental Fig. S5A) and PSI yields (Fig. 6C; Supplemental Fig. S5B) and, most importantly, the negligible net O_2 production (Fig. 3E) and CO_2 fixation rates (Fig. 7A; Supplemental Fig. S13A) on day 3. A residual PSII activity is ensured by circulating electrons in a water-water cycle. This was demonstrated by reduced PSII gross O_2 production (Fig. 7, A and C), which nearly equalled O_2 consumption in the light, resulting in practically zero net O_2 production. Since addition of an artificial PSII electron acceptor, DCBQ, largely restores O_2 evolving activity (Fig. 3E), a substantial portion of PSII centers are functional, but downstream electron flux is restricted. This could be due to a highly reduced PQ pool, which in turn affects the redox potential of Q_B and thus Q_A^- reoxidation (Haimovich-Dayan et al., 2011). However, far-red light, which specifically excites PSI and drains electrons from the PQ pool, did not accelerate Q_A^- reoxidation in photomixotrophically cultured wild type (Supplemental Fig. S9B). Thus, overreduction of the PQ pool cannot be the sole reason for the restricted downstream electron flux. Interestingly, the photomixotrophically cultured wild type resembles DCMU-treated cells in many ways: (1) far-red light illumination increases steady-state fluorescence (Fig. 3C; Supplemental Fig. S4); (2) transient rereduction and subsequent reoxidation of Cyt *f* under illumination is nearly absent, and Cyt *f* decay in darkness is slow (Fig. 5); (3) flash-induced decay of Q_A^- after 3 d exposure to Glc highly resembles the kinetics of DCMU-treated cells (Fig. 8B) and differs from kinetics observed

in the DBMIB-treated wild type (Supplemental Fig. S9B; Deák et al., 2014). These results suggest that photosynthetic electron flow from PSII to the PQ pool and Cyt b_6f is hindered. However, this is not simply due to a highly reduced PQ pool.

The gradual disconnection between PSII and Cyt b_6f and the resulting decrease in photosynthesis could be due to a spatial isolation of PSII, via rearrangement in the thylakoid, to another location. Rearrangement of thylakoid-localized complexes, specifically NDH-1 and SDH, has been observed in response to redox-regulated changes in the electron transport chain (Liu et al., 2012). Applying the same analogy to PSII, the highly reduced state of the PQ pool might trigger the complexes to arrange into a more sparse distribution during photomixotrophic growth. Although cyanobacterial thylakoids are densely packed membranes (Kaňa, 2013), lateral heterogeneity (Agarwal et al., 2010) and mobility of PSII (Casella et al., 2017) have been demonstrated.

Photomixotrophy Does Not Alter Photosynthetic Electron Transport in ΔCytM

Surprisingly, deletion of CytM reverses the downregulation of photosynthesis in photomixotrophy, resulting in a profile similar to that of wild-type and ΔCytM cells grown under photoautotrophic conditions. Importantly, ΔCytM demonstrated unrestricted electron flow between PSII, Cyt b_6f, and PSI. The rate of gross O_2 production (Fig. 7, A and E) was 10 times higher in ΔCytM cells compared to wild-type cells cultured under photomixotrophic conditions. In contrast to the photomixotrophically cultured wild type, ΔCytM showed a clear wave pattern in Cyt *f* kinetics upon dark-to-light transition and did not demonstrate slow rereduction of Cyt *f* in the dark (Fig. 5B) or PSI donor-side limitation (Supplemental Fig. S5C). Finally, the abundance of D1 (Fig. 3F), PsaB (Fig. 6B), and PetA and PetB (Supplemental Dataset S3), the core subunits of PSII, PSI, and Cyt b_6f, respectively, was higher in ΔCytM than in the wild type, although the PSI:PSII ratio was unaltered (Supplemental Fig. S11). As a consequence, the rate of net O_2 production and CO_2 consumption (Fig. 7A) was substantially higher in ΔCytM, demonstrating that deletion of CytM conserves photosynthetic activity and circumvents the inhibition of Q_A^- reoxidation in photomixotrophy.

The exact mechanism by which ΔCytM alleviates blockage of the electron transport pathway was not elucidated in this work, nor has an exact role for this protein been determined in previous studies. CytM has been suggested to play a role in transferring electrons from Cyt b_6f to Flv1/Flv3, limiting productivity but providing a possible alternative route for safely transferring electrons to O_2 (Hiraide et al., 2015). However, given the low midpoint potential of CytM, a large energy barrier would have to be overcome in order for electron transfer downstream of Cyt b_6f to occur (Cho et al., 2000). Moreover, we demonstrated that the absence of CytM does not decrease O_2 photoreduction driven by FDPs in ΔCox/Cyd/CytM (Fig. 7, A and F), thus excluding this possibility. Recently, a cyanobacterial ferredoxin, Fed2, was shown to play a role in iron sensing and regulation of the IsiA antenna protein, a protein that is typically expressed when cells are exposed to low-iron conditions (Schorsch et al., 2018). Similar to Fed2, it is possible that CytM plays a regulatory role in the cell, rather than being directly involved in electron transport under photomixotrophy.

Under conditions in which cells are exposed to Glc or other sugars, CytM may regulate carbon assimilation. ΔCytM demonstrates substantial growth under dark heterotrophic conditions (Hiraide et al., 2015). However, the majority of the known cyanobacteria cannot grow heterotrophically, indicating that the function of CytM extends beyond the modulation of heterotrophic growth (Bialek et al., 2016). Under photomixotrophic

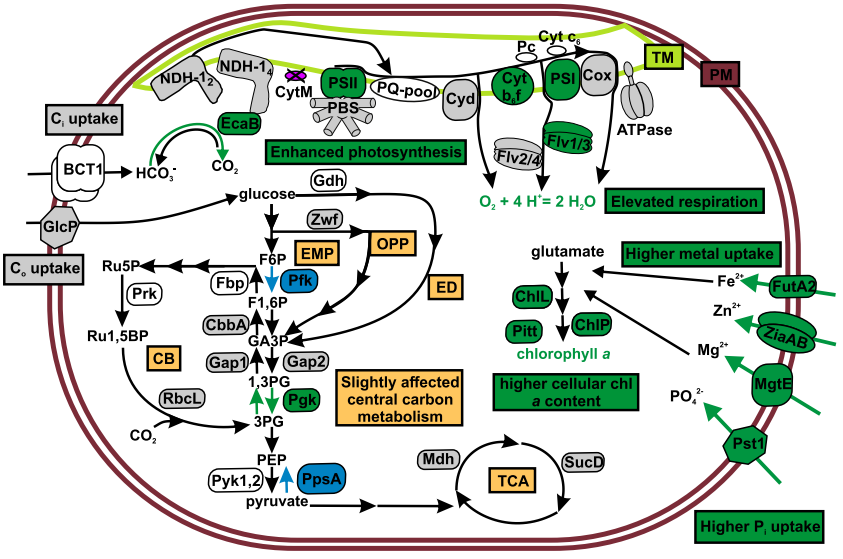

Figure 9. Schematic showing changes in the metabolism of photomixotrophically grown ΔCytM cells compared to the wild type. Proteins, compounds, and metabolic routes with increased abundance or activity in ΔCytM relative to the wild type are represented in green. Blue indicates lower abundance in ΔCytM, gray indicates no change, and white indicates undetermined abundance or activity. CB, Calvin-Benson cycle; C_i uptake, inorganic carbon uptake; C_o uptake, organic carbon uptake; ED, Entner-Doudoroff pathway; EMP, Embden-Meyerhof-Parnas pathway; OPP, oxidative pentose phosphate pathway; P_i uptake, inorganic phosphate uptake; PM, plasma membrane; TCA, tricarboxylic acid cycle; TM, thylakoid membrane.

conditions, CytM likely is involved in regulation of thylakoid rearrangements or photosynthetic electron transport and carbon fixation, limiting CO_2 uptake and decreasing the total amount of photosynthetic proteins, which in turn reduces photosynthesis. In line with this, we observed accumulation of EcaB in ΔCytM (Fig. 9; Supplemental Dataset S3). Enhanced EcaB levels likely result in greater inorganic carbon assimilation, higher carbon fixation, and increased turnover of NADPH, the terminal electron acceptor in linear photosynthetic electron transport. This in turn likely limits overreduction of the photosynthetic electron transport chain.

Regardless of the exact role of CytM, it is clear that deletion of this protein substantially increases growth of *Synechocystis* in photomixotrophy (Fig. 1), in line with previous studies (Hiraide et al., 2015). This is possibly due to an increase in photosynthetic capacity combined with efficient assimilation of Glc into central metabolism, resulting in greater biomass accumulation. This resulted in increased production of proteins required for enhanced growth, including those involved in phosphate uptake (PstA1, PstB1, PstB1′, and PstC; Supplemental Dataset S3), import of Mg^{2+} (MgtE), Zn^{2+} (ZiaA), and Fe^{2+} (FutA2), and production of chl (ChlP and ChlL; Fig. 9; Supplemental Dataset S3).

In conclusion, under long-term photomixotrophy *Synechocystis* cells gradually decrease photosynthetic electron transport by disconnecting PSII from Cyt b_6f. Deletion of CytM allows *Synechocystis* to maintain efficient photosynthesis and enhanced growth under long-term photomixotrophy. While we have not determined the exact function of CytM, we propose that it plays a role in reducing photosynthesis under conditions when both light intensity and Glc concentration fluctuate (Ittekkot et al., 1981; Hieronymi and Macke, 2010), and the redox state of the intertwined photosynthetic and respiratory electron transfer rapidly changes.

MATERIALS AND METHODS

Plasmid Construction

The genome sequence of *Synechocystis* sp. PCC 6803 released on November 5, 2004 was consulted via Cyanobase (http://genome.kazusa.or.jp/cyanobase) for primer design. Primers are listed in Supplemental Table S1. The *cytM* (*sll1245)* gene was deleted by amplifying a 906-bp fragment upstream of *cytM* using primers CytMleftfor and CytMleftrev and a 932-bp fragment downstream of *cytM* using primers CytMrightfor and CytMrightrev, followed by insertion of the respective fragments into the *Sac*I/*Eco*R1 and *Xba*I/*Bam*H1 sites of pUC19 to generate pCytM-1. The *Bam*H1-digested npt1/sacRB cassette from pUM24Cm (Ried and Collmer, 1987) was inserted into the *Bam*H1 site between the upstream and downstream fragments in pCytM-1 to generate pCytM-2.

Construction of *cytM* Deletion Mutants

Unmarked mutants of *Synechocystis* lacking *cytM* were constructed via a two-step homologous recombination protocol according to Lea-Smith et al. (2016b). To generate marked mutants, ~1 μg of plasmid pCytM-2 was mixed with *Synechocystis* cells for 6 h in liquid media, followed by incubation on BG-11 agar plates for ~24 h. An additional 3 mL of agar containing kanamycin was added to the surface of the plate, followed by further incubation for ~1 to 2 weeks. Transformants were subcultured to allow segregation of mutant alleles. Segregation was confirmed by PCR using primers CytMf and CytMr, which flank the deleted region. To remove the *npt*1/*sacRB* cassette to generate unmarked mutants, mutant lines were transformed with 1 μg of the markerless CytM-1 construct. Following incubation in BG-11 liquid media for 4 d and agar plates containing Suc for a further 1 to 2 weeks, transformants were patched on kanamycin and Suc plates. Suc resistant, kanamycin sensitive strains containing the unmarked deletion were confirmed by PCR using primers flanking the deleted region (Supplemental Fig. S2B). The ΔCox/Cyd/CytM unmarked strain was generated via the same method in the background of the unmarked ΔCox/Cyd strain (Lea-Smith et al., 2013).

Cultivation

Cells kept in cryogenic storage were revived on BG-11 agar plates at 3% (v/v) CO_2. Pre-experimental cultures were inoculated at 0.1 OD_{750} by transferring a patch of cells from plates into 30 mL BG-11 medium buffered with 10 mM TES-KOH (pH 8.2) in 100-mL Erlenmeyer flasks. Cultures were shaken at 120 rpm at 30°C and exposed to constant white fluorescent light of 50 μmol photons m^{-2} s^{-1} intensity in a Sanyo Environmental Test Chamber supplemented with 3% (v/v) CO_2. Pre-experimental cultures were cultivated for 3 d, with density typically reaching 2.5 ± 0.5 OD_{750}.

Experimental cultures for growth and photophysiological experiments were inoculated in 30 mL fresh BG-11 media at 0.1 OD_{750} from harvested pre-experimental cultures. The media was buffered with 10 mM TES-KOH (pH 8.2), the CO_2 concentration was atmospheric, and cultures were agitated in 100-mL Erlenmeyer flasks at 120 rpm in AlgaeTRON AG130 cool-white LED chambers (PSI Instruments). Growth was tested under constant light of 50 μmol photons m^{-2} with different initial Glc concentrations: (1) no Glc; (2) 5 mM Glc; and (3) 10 mM Glc. At 10 mM Glc, additional light regimes were tested: (4) 10 μmol photons m^{-2} s^{-1} light and (5) 15 min 50 μmol photons m^{-2} s^{-1} every 24 h. For photophysiological studies, cells were cultivated under condition 3 for 3 d. For proteomics analysis, cells were cultivated similarly to those in condition 3, with the exception of an extra 3-d-long precultivation step at atmospheric CO_2 without Glc.

Cell Counting, Cell Size Determination

Cell number was determined with a Nexcelom Cellometer X2 via the following method. Sample OD_{750} was adjusted to 1, brightfield images were captured, and the cell number was determined by the Nexcelom software. In order to exclude the visual glitches falsely recognized as cells by the software, only the four most populous cell-size groups were averaged. Typically, 3,000 cells were counted per plate.

Glc Determination

Glc concentration of the spent media was determined spectrophotometrically with the commercial High Sensitivity Glc Assay Kit (Sigma-Aldrich). Prior to measurements, the cell suspension was centrifuged at 5,000*g* for 10 min and the supernatant was filtered through a 0.2-μm filter.

MIMS Measurements

Gas fluxes of intact cells were measured using MIMS. The in-house-built system consists of a DW-1 oxygen electrode chamber (Hansatech) connected to the vacuum line of a MS (Prima PRO model, Thermo Scientific). The sample cuvette was separated from the vacuum line by a Hansatech S4 polytetrafluoroethylene membrane. Samples were pelleted and resuspended in fresh BG-11 supplemented by 10 mM Glc and buffered to pH 8.2 with 10 mM TES-KOH. Chl *a* concentration was adjusted to 10 μg mL^{-1}. Prior to measurements, the sample was enriched with 98% (v/v) $^{18}O_2$ heavy isotope (CK Isotopes), the dissolved total inorganic carbon concentration was adjusted to 1.5 mM by adding $NaHCO_3$, and 10 to 15 min dark adaptation was applied. The measurement was performed in a semiclosed cuvette at 30°C with constant stirring. The light source was a 150 Watt, 21 V, EKE quartz halogen-powered fiber-optic illuminator (Fiber-Lite DC-950, Dolan-Jenner). A two-point calibration was used to calibrate the O_2 signal in milli-Q water. Total inorganic carbon was calibrated by injecting known HCO_3^- samples into a known volume of growth media buffered to pH 8.2 with 10 mM TES-KOH. A mathematical offset

accounted for the changing concentration of the $^{18}O_2$ and $^{16}O_2$ isotopologues over the course of an experiment to enable the accurate determination of rates (Hoch and Kok, 1963). Rates were calculated as described previously (Beckmann et al., 2009).

Clark-Type Electrode Measurements

Net O_2 production of intact cells was tested in the presence of 0.5 mM DCBQ at 30°C with a Clark-type oxygen electrode and chamber (Hansatech). Prior to the measurements, cells were resuspended in BG-11 (pH 8.2) supplemented with 10 mM Glc, the chl *a* concentration was adjusted to 7.5 μg mL^{-1}, then the samples were dark adapted for 1 to 2 min. O_2 production was initiated by 1,000 μmol photons m^{-2} s^{-1} white light using a Fiber-Lite DC-950 light source. Rates of oxygen production were calculated using the Hansatech software.

Chl Fluorescence and P700 Oxidoreduction Measurements

Whole-cell chl fluorescence was measured simultaneously with P700 with a pulse amplitude-modulated fluorometer (Dual-PAM-100). Prior to measurements, cells were resuspended in BG-11 (pH 8.2) supplemented with 10 mM Glc, and the chl *a* concentration was adjusted to 15 μg mL^{-1}. Measurements were performed at 30°C, and samples were initially incubated in darkness for 15 min with stirring. To determine P_m, 30 s strong far-red light (720 nm, 40 W m^{-2}) and red MT saturating pulses were applied. MT pulses were set to an intensity of 5,000 μmol photons m^{-2} s^{-1} (width 500 ms). Red (635 nm) actinic light of 50 μmol photons m^{-2} s^{-1} intensity was used as background illumination. Photosynthetic parameters were calculated as described previously (Klughammer et al., 2008a, 2008b).

Relaxation of flash-induced fluorescence yield was monitored using a fluorometer (FL3500, PSI Instruments), as outlined previously (Allahverdiyeva et al., 2013). Prior to the measurement, cells were resuspended in BG-11 (pH 8.2) supplemented with 10 mM Glc, adjusted to 5 μg chl *a* mL^{-1} and dark adapted for 5 min. Curves were referenced against F_0 and normalized to F_m.

Measurement of Cytochrome *f* Redox Kinetics

Cyt *f* redox kinetics were determined in intact cells by deconvoluting absorbance changes at 546, 554, 563, and 573 nm that were measured using a JTS-10 pump probe spectrophotometer (BioLogic) and appropriate 10 nm FWHM interference filters. BG39 filters (Schott) were used to shield the light detectors from scattered light. Deconvolution was performed with the JTS-10 software. Prior to the experiments, cells were harvested and chl *a* concentration was adjusted to 5 μg mL^{-1} by resuspension in fresh BG-11 with or without 10 mM Glc. Cells were dark adapted for 2 min prior to measurements with each interference filter, and then illuminated with green light of 500 μmol photons m^{-2} s^{-1} intensity for 5 s. Flashes of white detection light were administered during 200-μs dark intervals in actinic illumination. When appropriate, 20 μM DCMU was added to the samples before dark adaptation.

Western Blotting

Total protein extraction, electrophoresis, and immunoblotting were performed as described previously (Huokko et al., 2019). Antibodies raised against PsaB (AS10 695, Agrisera), D1 (AS11 1786, Agrisera), and Flv3 (Antiprot) were used in this study.

MS Analysis: Sample Preparation, Data-Dependent Analysis, Protein Identification and Quantitation

For data analysis, we used the proteome of *Synechocystis* sp. 6803 substrain Kazusa sequenced in 2004. Protein annotation was downloaded from Uniprot and Cyanobase. Hydrophobicity was determined via the grand average of hydropathy (GRAVY) index at www.gravy-calculator.de, and pI was calculated via https://web.expasy.org/compute_pi/.

Sample preparation for MS, data-dependent analysis, and protein identification was performed as detailed previously (Huokko et al., 2019). The MS proteomics data were deposited to the ProteomeXchange Consortium via the PRIDE partner repository with the dataset identifier PXD015246 and 10.6019/PXD015246 (Perez-Riverol et al., 2019).

Statistical Analysis

P-values were calculated by one-way ANOVA and differences in the data were considered statistically significant at $P < 0.05$.

Accession Numbers

Gene/protein names and accession numbers of all genes/proteins identified in this study are listed in Supplemental Dataset S1. The MS proteomics data were deposited to the ProteomeXchange Consortium via the PRIDE partner repository with the dataset identifier PXD015246 and 10.6019/PXD015246 (Perez-Riverol et al., 2019).

Supplemental Data

The following supplemental materials are available.

Supplemental Figure S1. Alignment of CytM from sequenced cyanobacterial species.

Supplemental Figure S2. Generation of *cytM* deletion mutants in *Synechocystis*.

Supplemental Figure S3. Cell size of wild type and ΔCytM grown photomixotrophically and photoautotrophically.

Supplemental Figure S4. Fluorescence transients of photoautotrophically cultivated wild type and ΔCytM determined in the presence of 2 μM DCMU.

Supplemental Figure S5. Photosynthetic parameters of wild type and ΔCytM grown photomixotrophically and photoautotrophically.

Supplemental Figure S6. Fluorescence transients and P700 oxidoreduction on day 3 of photomixotrophic growth of the wild-type *Synechocystis* substrain.

Supplemental Figure S7. Fluorescence transients and P700 oxidoreduction kinetics of photomixotrophically grown wild type, ΔCytM, ΔCox/Cyd, and ΔCox/Cyd/CytM.

Supplemental Figure S8. Fluorescence transients and P700 oxidoreduxtion kinetics of photoautotrophically grown wild type, ΔCytM, ΔCox/Cyd, and ΔCox/Cyd/CytM.

Supplemental Figure S9. Flash-induced increase of fluorescence yield and its relaxation in dark in photoautotrophically grown wild type and ΔCytM.

Supplemental Figure S10. Redox kinetics of Cyt *f* in photoautotrophically grown ΔCytM cells.

Supplemental Figure S11. 77K steady-state fluorescence emission spectra of wild type and ΔCytM grown photomixotrophically.

Supplemental Figure S12. Fast kinetics of P700 oxidoreduction of wild type and ΔCytM grown under photoautotrophic conditions.

Supplemental Figure S13. The rate of CO_2 fluxes in photomixotrophically grown wild type, ΔCytM, ΔCox/Cyd, and ΔCox/Cyd/CytM.

Supplemental Table S1. List of oligonucleotides used in this study.

Supplemental Table S2. Rates of O_2 and CO_2 fluxes in photomixotrophically grown wild type, ΔCytM, ΔCox/Cyd, and ΔCox/Cyd/CytM.

Supplemental Dataset S1. Proteins identified by data-dependent analysis in photomixotrophically grown wild type and ΔCytM.

Supplemental Dataset S2. Differentially expressed proteins in photomixotrophically grown ΔCytM versus the wild type.

Supplemental Dataset S3. A selection of differentially expressed proteins in photomixotrophically cultured ΔCytM compared to the wild type.

ACKNOWLEDGMENTS

We thank Steffen Grebe for helping with Dual-PAM measurements and Ville Käpylä for laboratory assistance. MS analysis was performed at the Turku

Proteomics Facility hosted by the University of Turku and Åbo Akademi University, supported by Biocenter Finland.

Received March 6, 2020; accepted March 23, 2020; published April 21, 2020.

LITERATURE CITED

Agarwal R, Matros A, Melzer M, Mock H-P, Sainis JK (2010) Heterogeneity in thylakoid membrane proteome of *Synechocystis* 6803. J Proteomics **73:** 976–991

Allahverdiyeva Y, Isojärvi J, Zhang P, Aro E-M (2015) Cyanobacterial oxygenic photosynthesis is protected by flavodiiron proteins. Life (Basel) **5:** 716–743

Allahverdiyeva Y, Mustila H, Ermakova M, Bersanini L, Richaud P, Ajlani G, Battchikova N, Cournac L, Aro E-M (2013) Flavodiiron proteins Flv1 and Flv3 enable cyanobacterial growth and photosynthesis under fluctuating light. Proc Natl Acad Sci USA **110:** 4111–4116

Badger MR, Palmqvist K, Yu J-W (1994) Measurement of CO_2 and HCO_3^- fluxes in cyanobacteria and microalgae during steady-state photosynthesis. Physiol Plant **90:** 529–536

Baers LL, Breckels LM, Mills LA, Gatto L, Deery M, Stevens TJ, Howe CJ, Lilley KS, Lea-Smith DJ (2019) Proteome mapping of a cyanobacterium reveals distinct compartment organisation and cell-dispersed metabolism. Plant Physiol **181:** 1721–1738

Beckmann K, Messinger J, Badger MR, Wydrzynski T, Hillier W (2009) On-line mass spectrometry: Membrane inlet sampling. Photosynth Res **102:** 511–522

Bernroitner M, Tangl D, Lucini C, Furtmüller PG, Peschek GA, Obinger C (2009) Cyanobacterial cytochrome c_M: Probing its role as electron donor for Cu_A of cytochrome *c* oxidase. Biochim Biophys Acta **1787:** 135–143

Bialek W, Nelson M, Tamiola K, Kallas T, Szczepaniak A (2008) Deeply branching c_6-like cytochromes of cyanobacteria. Biochemistry **47:** 5515–5522

Bialek W, Szczepaniak A, Kolesinski P, Kallas T (2016) Cryptic c_6-like and c_M cytochromes of cyanobacteria. In WA Kramer, and T Kallas, eds, Cytochrome Complexes: Evolution, Structures, Energy Transduction, and Signaling. Springer, Dordrecht, pp 713–734

Brown KA, Guo Z, Tokmina-Lukaszewska M, Scott LW, Lubner CE, Smolinski S, Mulder DW, Bothner B, King PW (2019) The oxygen reduction reaction catalyzed by *Synechocystis* sp. PCC 6803 flavodiiron proteins. Sustain Energy Fuels **3:** 3191–3200

Büsch A, Friedrich B, Cramm R (2002) Characterization of the *norB* gene, encoding nitric oxide reductase, in the nondenitrifying cyanobacterium *Synechocystis* sp. strain PCC6803. Appl Environ Microbiol **68:** 668–672

Casella S, Huang F, Mason D, Zhao G-Y, Johnson GN, Mullineaux CW, Liu L-N (2017) Dissecting the native architecture and dynamics of cyanobacterial photosynthetic machinery. Mol Plant **10:** 1434–1448

Chandramouli K, Qian P-Y (2009) Proteomics: Challenges, techniques and possibilities to overcome biological sample complexity. Hum Genomics Proteomics **2009:** 239204

Cho YS, Pakrasi HB, Whitmarsh J (2000) Cytochrome c_M from *Synechocystis* 6803. Detection in cells, expression in *Escherichia coli*, purification and physical characterization. Eur J Biochem **267:** 1068–1074

Deák Z, Sass L, Kiss E, Vass I (2014) Characterization of wave phenomena in the relaxation of flash-induced chlorophyll fluorescence yield in cyanobacteria. Biochim Biophys Acta **1837:** 1522–1532

Durán RV, Hervás M, De La Rosa MA, Navarro JA (2004) The efficient functioning of photosynthesis and respiration in *Synechocystis* sp. PCC 6803 strictly requires the presence of either cytochrome c_6 or plastocyanin. J Biol Chem **279:** 7229–7233

Ermakova M, Huokko T, Richaud P, Bersanini L, Howe CJ, Lea-Smith DJ, Peltier G, Allahverdiyeva Y (2016) Distinguishing the roles of thylakoid respiratory terminal oxidases in the cyanobacterium *Synechocystis* sp. PCC 6803. Plant Physiol **171:** 1307–1319

Haimovich-Dayan M, Kahlon S, Hihara Y, Hagemann M, Ogawa T, Ohad I, Lieman-Hurwitz J, Kaplan A (2011) Cross-talk between photomixotrophic growth and CO_2-concentrating mechanism in *Synechocystis* sp. strain PCC 6803. Environ Microbiol **13:** 1767–1777

Helman Y, Tchernov D, Reinhold L, Shibata M, Ogawa T, Schwarz R, Ohad I, Kaplan A (2003) Genes encoding A-type flavoproteins are essential for photoreduction of O_2 in cyanobacteria. Curr Biol **13:** 230–235

Hieronymi M, Macke A (2010) Spatiotemporal underwater light field fluctuations in the open ocean. J Eur Opt Soc Rapid Publ **5:** 10019s

Hiraide Y, Oshima K, Fujisawa T, Uesaka K, Hirose Y, Tsujimoto R, Yamamoto H, Okamoto S, Nakamura Y, Terauchi K, et al (2015) Loss of cytochrome c_M stimulates cyanobacterial heterotrophic growth in the dark. Plant Cell Physiol **56:** 334–345

Hoch G, Kok B (1963) A mass spectrometer inlet system for sampling gases dissolved in liquid phases. Arch Biochem Biophys **101:** 160–170

Huokko T, Muth-Pawlak D, Aro E-M (2019) Thylakoid localized type 2 NAD(P)H dehydrogenase NdbA optimizes light-activated heterotrophic growth of *Synechocystis* sp. PCC 6803. Plant Cell Physiol **60:** 1386–1399

Huokko T, Muth-Pawlak D, Battchikova N, Allahverdiyeva Y, Aro EM (2017) Role of type 2 NAD(P)H dehydrogenase NdbC in redox regulation of carbon allocation in *Synechocystis*. Plant Physiol **174:** 1863–1880

Ittekkot V, Brockmann U, Michaelis W, Degens E (1981) Dissolved free andcCombined carbohydrates during a phytoplankton bloom in the northern North Sea. Mar Ecol Prog Ser **4:** 299–305

Kaňa R (2013) Mobility of photosynthetic proteins. Photosynth Res **116:** 465–479

Kerfeld CA, Krogmann DW (1998) Photosynthetic cytochromes *c* in cyanobacteria, algae, and plants. Annu Rev Plant Physiol Plant Mol Biol **49:** 397–425

Klughammer C, Schreiber U (2008a) Complementary PS II quantum yields calculated from simple fluorescence parameters measured by PAM fluorometry and the saturation pulse method. PAM Appl Notes **1:** 27–35

Klughammer C, Schreiber U (2008b) Saturation Pulse method for assessment of energy conversion in PS I. PAM Appl Notes **1:** 11–14

Kranzler C, Lis H, Finkel OM, Schmetterer G, Shaked Y, Keren N (2014) Coordinated transporter activity shapes high-affinity iron acquisition in cyanobacteria. ISME J **8:** 409–417

Lea-Smith DJ, Bombelli P, Vasudevan R, Howe CJ (2016a) Photosynthetic, respiratory and extracellular electron transport pathways in cyanobacteria. Biochim Biophys Acta Bioenerg **1857:** 247–255

Lea-Smith DJ, Ross N, Zori M, Bendall DS, Dennis JS, Scott SA, Smith AG, Howe CJ (2013) Thylakoid terminal oxidases are essential for the cyanobacterium *Synechocystis* sp. PCC 6803 to survive rapidly changing light intensities. Plant Physiol **162:** 484–495

Lea-Smith DJ, Vasudevan R, Howe CJ (2016b) Generation of marked and markerless mutants in model cyanobacterial species. J Vis Exp (111): e54001

Lee S, Ryu J-Y, Kim SY, Jeon J-H, Song JY, Cho H-T, Choi S-B, Choi D, de Marsac NT, Park Y-I (2007) Transcriptional regulation of the respiratory genes in the cyanobacterium *Synechocystis* sp. PCC 6803 during the early response to glucose feeding. Plant Physiol **145:** 1018–1030

Liu L-N, Bryan SJ, Huang F, Yu J, Nixon PJ, Rich PR, Mullineaux CW (2012) Control of electron transport routes through redox-regulated redistribution of respiratory complexes. Proc Natl Acad Sci USA **109:** 11431–11436

Malakhov MP, Malakhova OA, Murata N (1999) Balanced regulation of expression of the gene for cytochrome cM and that of genes for plastocyanin and cytochrome c6 in *Synechocystis*. FEBS Lett **444:** 281–284

Malakhov MP, Wada H, Los DA, Semenenko VE, Murata N (1994) A new type of cytochrome *c* from *Synechocystis* PCC6803. J Plant Physiol **144:** 259–264

Manna P, Vermaas W (1997) Lumenal proteins involved in respiratory electron transport in the cyanobacterium *Synechocystis* sp. PCC6803. Plant Mol Biol **35:** 407–416

Molina-Heredia FP, Balme A, Hervás M, Navarro JA, De la Rosa MA (2002) A comparative structural and functional analysis of cytochrome c_M cytochrome c_6 and plastocyanin from the cyanobacterium *Synechocystis* sp. PCC 6803. FEBS Lett **517:** 50–54

Moore LR (2013) More mixotrophy in the marine microbial mix. Proc Natl Acad Sci USA **110:** 8323–8324

Mullineaux CW (2014) Co-existence of photosynthetic and respiratory activities in cyanobacterial thylakoid membranes. Biochim Biophys Acta **1837:** 503–511

Mustila H, Paananen P, Battchikova N, Santana-Sánchez A, Muth-Pawlak D, Hagemann M, Aro E-M, Allahverdiyeva Y (2016) The flavodiiron protein Flv3 functions as a homo-oligomer during stress acclimation and is distinct from the Flv1/Flv3 hetero-oligomer specific to the O2 photoreduction pathway. Plant Cell Physiol **57:** 1468–1483

Ogawa T (1991) A gene homologous to the subunit-2 gene of NADH dehydrogenase is essential to inorganic carbon transport of *Synechocystis* PCC6803. Proc Natl Acad Sci USA **88:** 4275–4279

Perez-Riverol Y, Csordas A, Bai J, Bernal-Llinares M, Hewapathirana S, Kundu DJ, Inuganti A, Griss J, Mayer G, Eisenacher M, et al (2019) The PRIDE database and related tools and resources in 2019: Improving support for quantification data. Nucleic Acids Res **47**(D1): D442–D450

Pils D (1997) Evidence for in vivo activity of three distinct respiratory terminal oxidases in the cyanobacterium *Synechocystis* sp. strain PCC6803. FEMS Microbiol Lett **152:** 83–88

Ried JL, Collmer A (1987) An *nptI-sacB-sacR* cartridge for constructing directed, unmarked mutations in gram-negative bacteria by marker exchange-eviction mutagenesis. Gene **57:** 239–246

Santana-Sanchez A, Solymosi D, Mustila H, Bersanini L, Aro E-M, Allahverdiyeva Y (2019) Flavodiiron proteins 1-to-4 function in versatile combinations in O_2 photoreduction in cyanobacteria. eLife **8:** e45766

Schorsch M, Kramer M, Goss T, Eisenhut M, Robinson N, Osman D, Wilde A, Sadaf S, Brückler H, Walder L, et al (2018) A unique ferredoxin acts as a player in the low-iron response of photosynthetic organisms. Proc Natl Acad Sci USA **115:** E12111–E12120

Schottkowski M, Ratke J, Oster U, Nowaczyk M, Nickelsen J (2009) Pitt, a novel tetratricopeptide repeat protein involved in light-dependent chlorophyll biosynthesis and thylakoid membrane biogenesis in *Synechocystis* sp. PCC 6803. Mol Plant **2:** 1289–1297

Schuller JM, Birrell JA, Tanaka H, Konuma T, Wulfhorst H, Cox N, Schuller SK, Thiemann J, Lubitz W, Sétif P, et al (2019) Structural adaptations of photosynthetic complex I enable ferredoxin-dependent electron transfer. Science **363:** 257–260

Schultze M, Forberich B, Rexroth S, Dyczmons NG, Roegner M, Appel J (2009) Localization of cytochrome b_6f complexes implies an incomplete respiratory chain in cytoplasmic membranes of the cyanobacterium *Synechocystis* sp. PCC 6803. Biochim Biophys Acta **1787:** 1479–1485

Shen JR, Inoue Y (1993) Binding and functional properties of two new extrinsic components, cytochrome *c*-550 and a 12-kDa protein, in cyanobacterial photosystem II. Biochemistry **32:** 1825–1832

Shpilyov AV, Zinchenko VV, Shestakov SV, Grimm B, Lokstein H (2005) Inactivation of the geranylgeranyl reductase (ChlP) gene in the cyanobacterium *Synechocystis* sp. PCC 6803. Biochim Biophys Acta **1706:** 195–203

Smith AJ (1983) Modes of cyanobacterial carbon metabolism. Ann Microbiol (Paris) **134B:** 93–113

Sonoda M, Kitano K, Katoh A, Katoh H, Ohkawa H, Ogawa T (1997) Size of cotA and identification of the gene product in *Synechocystis* sp. strain PCC6803. J Bacteriol **179:** 3845–3850

Srivastava A, Strasser RJ, Govindjee (1995) Differential effects of dimethylbenzoquinone and dichlorobenzoquinone on chlorophyll fluorescence transient in spinach thylakoids. J Photochem Photobiol B **31:** 163–169

Stal LJ, Moezelaar R (1997) Fermentation in cyanobacteria. FEMS Microbiol Rev **21:** 179–211

Sültemeyer D, Price GD, Yu J-W, Badger MR (1995) Characterisation of carbon dioxide and bicarbonate transport during steady-state photosynthesis in the marine cyanobacterium *Synechococcus* strain PCC7002. Planta **197:** 597–607

Sun N, Han X, Xu M, Kaplan A, Espie GS, Mi H (2018) A thylakoid-located carbonic anhydrase regulates CO 2 uptake in the cyanobacterium *Synechocystis* sp. PCC 6803. New Phytol **222:** 206–217

Takahashi H, Uchimiya H, Hihara Y (2008) Difference in metabolite levels between photoautotrophic and photomixotrophic cultures of *Synechocystis* sp. PCC 6803 examined by capillary electrophoresis electrospray ionization mass spectrometry. J Exp Bot **59:** 3009–3018

Teeling H, Fuchs BM, Becher D, Klockow C, Gardebrecht A, Bennke CM, Kassabgy M, Huang S, Mann AJ, Waldmann J, et al (2012) Substrate-controlled succession of marine bacterioplankton populations induced by a phytoplankton bloom. Science **336:** 608–611

Vermaas WFJ 2001. Photosynthesis and respiration in cyanobacteria. eLS doi:10.1038/npg.els.0001670

Vicente JB, Gomes CM, Wasserfallen A, Teixeira M (2002) Module fusion in an A-type flavoprotein from the cyanobacterium *Synechocystis* condenses a multiple-component pathway in a single polypeptide chain. Biochem Biophys Res Commun **294:** 82–87

Wegener KM, Welsh EA, Thornton LE, Keren N, Jacobs JM, Hixson KK, Monroe ME, Camp DG II, Smith RD, Pakrasi HB (2008) High sensitivity proteomics assisted discovery of a novel operon involved in the assembly of photosystem II, a membrane protein complex. J Biol Chem **283:** 27829–27837

Willows RD, Mayer SM, Foulk MS, DeLong A, Hanson K, Chory J, Beale SI (2000) Phytobilin biosynthesis: The *Synechocystis* sp. PCC 6803 heme oxygenase-encoding *ho1* gene complements a phytochrome-deficient *Arabidopsis thaliana hy1* mutant. Plant Mol Biol **43:** 113–120

Wu Q, Vermaas WF (1995) Light-dependent chlorophyll a biosynthesis upon chlL deletion in wild-type and photosystem I-less strains of the cyanobacterium *Synechocystis* sp. PCC 6803. Plant Mol Biol **29:** 933–945

Zilliges Y, Dau H (2016) Unexpected capacity for organic carbon assimilation by *Thermosynechococcus elongatus*, a crucial photosynthetic model organism. FEBS Lett **590:** 962–970

Zubkov MV, Tarran GA (2008) High bacterivory by the smallest phytoplankton in the North Atlantic Ocean. Nature **455:** 224–226